Non-Contrast Magnetic Resonance Angiography: Techniques, Principles, and Applications

Ananya Panda, MBBS, MD, FRCR[a], Christopher J. Francois, MD[b], Candice A. Bookwalter, MD[b], Abhishek Chaturvedi, MD[c], Jeremy D. Collins, MD[b], Tim Leiner, MD, PhD[b], Prabhakar Shantha Rajiah, MBBS, MD, FRCR[b,*]

KEYWORDS

• Magnetic resonance • Non-contrast angiography • Magnetic resonance angiography • Renal artery • Peripheral artery • Pulmonary • Cerebral • Flow measurement

KEY POINTS

- Various techniques can be used to perform bright-blood (BB) non-contrast magnetic resonance angiography (MRA), each with preferred clinical utility and limitations.
- Balanced steady-state free-precession (b-SSFP) imaging is a rapid technique based on the intrinsically high T2/T1 ratio of blood that provides simultaneous visualization of arteries and veins.
- Time-of-flight MRA relies on inflow-related enhancement and is most widely used for neurovascular imaging.
- Cardiac phase-dependent, flow-based techniques include subtractive fast spin-echo, Quiescent Interval Steady-State, and three-dimensional b-SSFP with flow-sensitive dephasing, which are typically used for peripheral extremity angiography.
- Phase-contrast MRA are velocity-sensitive techniques that can provide both anatomic information and flow quantification.
- Arterial spin labeling MRA is widely used for renal MRA, and can be further tailored for the evaluation of cerebral, carotid, hepatic, and pulmonary circulations.
- New multi-contrast techniques allow simultaneous evaluation of vessel wall (black-blood) and luminal (bight blood), and is useful for carotid and cardiovascular imaging.

INTRODUCTION

Both contrast-enhanced magnetic resonance angiography (CE-MRA) and non-contrast-MRA are widely used in clinical practice to assess the presence, location, and extent of vascular involvement in a variety of conditions. Unlike computed tomography (CT) angiography, delineation of vascular patency is not affected by dense mural calcifications in MRA. Although CE-MRA provides excellent information on vascular anatomy and temporal enhancement kinetics, there has been an increasing focus on developing non-contrast MRA techniques. These developments are motivated by patient comfort, decreased cost as well as the potential risks of nephrogenic systemic fibrosis in patients with acute kidney injury or Grade 4 and Grade 5 chronic kidney disease.[1–3] The clinical need for robust MRA studies

[a] Department of Radiology, All India Institute of Medical Sciences, Jodhpur, India; [b] Department of Radiology, Mayo Clinic, Rochester, MN, USA; [c] Department of Radiology, University of Rochester Medical Center, Rochester, NY, USA
* Corresponding author.
E-mail address: radpry3@gmail.com

Magn Reson Imaging Clin N Am 31 (2023) 337–360
https://doi.org/10.1016/j.mric.2023.04.001
1064-9689/23/© 2023 Elsevier Inc. All rights reserved.
Descargado para Anonymous User (n/a) en National Library of Health and Social Security de ClinicalKey.es por Elsevier en julio 13, 2023. Para uso personal exclusivamente. No se permiten otros usos sin autorización. Copyright ©2023. Elsevier Inc. Todos los derechos reservados.

is also greatest in patients with chronic kidney disease and related comorbidities (eg, atherosclerosis, diabetes, peripheral vascular disease). In these patient sub-groups, non-contrast MRA can provide a safe, contrast-free, and completely non-invasive imaging workup. Non-contrast MRA may also be preferred in pregnant women and in younger patients who may need repeated CE examinations as MRA exams are not associated with radiation and the long-term effects of gadolinium deposition in brain, bones, and cerebrospinal fluid are not known.[4–6] Although the iron-based contrast agent ferumoxytol is an alternative for CE-MRA, it is more expensive, has a higher anaphylactic risk, and is currently not Food and Drug Adminstration (FDA)-approved for CE-MRA in the United States.[7] Non-contrast MRA avoids all associated costs and adverse risks associated with contrast administration.[8] Non-contrast MRA is also independent of bolus timing, and therefore, can be repeated multiple times, albeit at the cost of increased examination time. Non-contrast MRA may be performed pre- or post-contrast as part of a standard protocol or added on the fly if there are technical issues in the initial CE-MRA acquisition due to contrast bolus mistiming issues. In such cases, non-contrast MRA can provide complementary information to CE-MRA.

Despite the benefits of non-contrast MRA, these techniques have been historically underutilized compared to CE-MRA, due to the lower spatial resolution and signal-to-noise ratio (SNR), longer scan times, and greater artifacts. However, multiple developments in scanner hardware, including multi-receiver phased-array coils for parallel imaging, faster and stronger gradients, and higher magnetic field strengths enable non-contrast MRA with improved SNR in clinically acceptable scan times.[9] Non-Cartesian sampling techniques, compressed sensing, and deep learning for denoising and image reconstruction have the potential to further improve the quality and speed of non-contrast MRA exams.[10,11] Although both bright-blood (BB) and black-blood imaging can be considered non-contrast MRA techniques, this review focuses on various BB non-contrast MRA techniques, their principles, contrast mechanisms, and relevant clinical applications.

NON-CONTRAST MAGNETIC RESONANCE ANGIOGRAPHY TECHNIQUES

Non-contrast MRA techniques can be broadly classified based on the dominant contrast mechanism used to produce images (**Table 1**). In non-contrast MRA, the visualization of blood vessels is based on utilizing the (a) properties of blood flow and velocity or the (b) intrinsic high T1 and T2 relaxation times of blood. These properties are combined with background suppression techniques, flow-encoding or flow-dephasing gradients, and flow-compensated readouts to produce MRA images.[11–13]

Table 1
Mechanisms of non-contrast magnetic resonance angiography techniques

Dominant Contrast Mechanism	Non-contrast MRA Technique
Intrinsic high T2/T1 ratio of blood (flow-independent MRA)	• b-SSFP (balanced steady-state free precession)
Blood-inflow-based	• Time-of-flight (TOF) • Quiescent Interval Slice-Selective (QISS) • Inflow-Dependent Inversion Recovery (IFDIR)
Cardiac phase-dependent, flow-based	• Subtractive 3D fast spin-echo (FSE) • 3D-b-SSFP with flow-sensitive dephasing (FSD)
Velocity sensitive techniques	• Phase-contrast (PC)-MRA: 3D or 4D flow imaging • Velocity –selective MRA
Arterial spin labeling (ASL)	• Flow-in ASL • Flow-out ASL • Alternate tag On/Off subtractive MRA
Multi-contrast techniques	• Simultaneous non-contrast angiography (SNAP) • MTC-BOOST

BALANCED STEADY-STATE FREE PRECESSION

Principle

Balanced steady-state free-precession (b-SSFP) MRA is a gradient-echo technique based on the long T1 and T2 relaxation times of blood and its high T2/T1 ratio, which produces BB images with high vessel-to-background contrast.[12] For a three-dimensional (3D)-slab acquisition, imaging is performed by applying a series of equally spaced alternating radiofrequency (RF) pulses in all three axes, such that a coherent steady-state with balanced longitudinal and transverse magnetization is produced after many repetition times

Descargado para Anonymous User (n/a) en National Library of Health and Social Security de ClinicalKey.es por Elsevier en julio 13, 2023. Para uso personal exclusivamente. No se permiten otros usos sin autorización. Copyright ©2023. Elsevier Inc. Todos los derechos reservados.

(TRs). The signal intensity of the resultant image is dependent on the T2/T1 ratio. The TR is kept as short as possible (typically <5 msec on modern MR systems, but much less than the T2 relaxation time of blood) to minimize signal loss due to the dephasing of transverse magnetization. The readout is acquired such that the time of echo (TE) and free induction decay (FID) coincide in the middle of the TR (TR/2) (**Fig. 1**). Background fat suppression is applied at the time of readout, as fat has a similarly high T2/T1 ratio. For additional background tissue and venous suppression, a T2 prep pulse or DIXON technique may also be used.[9,12,14,15] Because of the symmetric nature of applied gradients, this technique is flow-compensated which is also advantageous for other non-contrast MRA techniques, as described later. Using a breath-hold acquisition or free breathing with navigator gating can mitigate respiratory motion in the thorax and abdomen.[14] For coronary MRA, additional electrocardiogram (ECG)-gating is also used and images are acquired in mid-late diastole to reduce pulsation artifacts (**Fig. 2**).[16,17]

Intrinsic high SNR and lack of reliance on blood flow make this sequence ideal for imaging slow flow (including venous flow), and in areas where background anatomic information is useful (eg, thoracic and abdominal imaging).[18] The sequence can also cover a large field of view with relatively short scan times.[9]

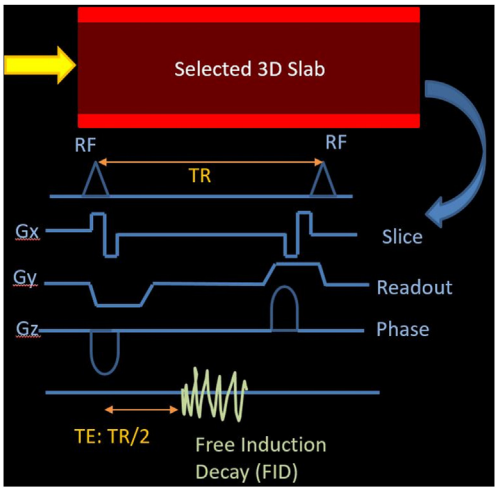

Fig. 1. Schematic of 3D-b-SSFP sequence. Multiple radiofrequency (RF) pulses are applied at short time of repetition (TRs). Balanced gradients are applied in all three axes (x, y, z) such that FID and TE coincide in the middle of TR. Coherent steady-state is attained after many such repetitions and signals are combined from multiple TRs to produce BB MRA images. Due to symmetric gradients, the sequence is flow-compensated and the final bright signal in the vessels is due to the high T2/T1 ratio of blood. Fat suppression techniques or DIXON are used for background fat suppression.

Limitations

Balanced SSFP is very sensitive to off-resonance artifacts often occurring at the ends of a large field of views (Moire' fringe artifacts). It is also prone to susceptibility artifacts due to metallic hardware (eg, vascular stents, clips, hardware, implantable cardiac devices, prosthetic valves) and air-tissue interfaces (eg, bowel, lungs) (**Fig. 3**). These can be partially mitigated by improved shimming, and are less obtrusive at lower field strengths.[9] Due to the short out-of-phase TE, there can be India ink artifacts from chemical shift imaging effect at fat–water interfaces, which can limit the detectability of mural thrombi and plaques.[14] As this sequence is independent of flow velocity, concomitant visualization of venous vasculature may be considered as unwanted venous contamination if the clinical question is only arterial imaging.

Common Clinical Applications

Balanced SSFP MRA is widely used for cardiothoracic, pulmonary, coronary, and abdominal MRA (**Fig. 4**).[19,20] It can also be combined with retrospective ECG-gated cine acquisition to visualize aortic and pulmonary outflow dynamics.[14,21] In body imaging, it has been used for visualization of hepatoportal, renal, and pelvic vasculature.[22–24] This technique has also been applied for lower extremity MRA and MR venograms (MRV) in combination with DIXON-based fat/water separation.[25]

TIME-OF-FLIGHT

Principle

Time-of-flight (TOF) MRA is the oldest and most widely used non-contrast BB MRA technique. It is based on the principle of inflow-related enhancement, that is, when unsaturated moving spins flow into a pre-selected slice that has been saturated by multiple RF excitations, these moving spins produce a bright signal in contrast to the stationary spins in the background saturated tissue. Additional spatial saturation pulses can be applied below or above the selected slice to suppress unwanted arterial and/or venous flow.[12] The placement of spatial saturation pulse depends on the anatomy and direction of unwanted flow. For example, in head and neck MRA, the spatial saturation pulse is applied above the selected slice to suppress unwanted venous inflow, or applied below the selected slice to suppress unwanted arterial inflow for MRV (**Fig. 5**). Conversely for

Descargado para Anonymous User (n/a) en National Library of Health and Social Security de ClinicalKey.es por Elsevier en julio 13, 2023. Para uso personal exclusivamente. No se permiten otros usos sin autorización. Copyright ©2023. Elsevier Inc. Todos los derechos reservados.

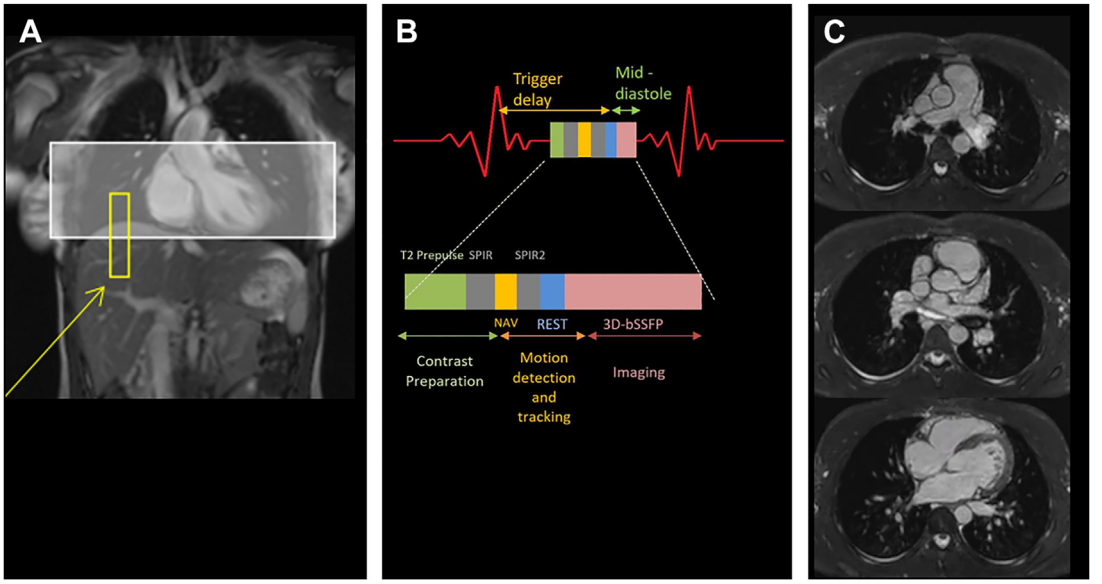

Fig. 2. 3D-b-SSFP sequence as modified for cardiac MRA. (*A*) Depicts placement of 3D slab (*white box*) for 3D-cardiac MRA. The yellow box (*yellow arrow*) denotes placement of the navigator gating slab over the right diaphragm for free breathing acquisition. (*B*) Depicts typical sequence design. In this example, a T2 prep pulse is used to saturate myocardium for visualization of coronary arteries. Fat suppression is obtained with Spectral Presaturation with Inversion Recovery (SPIR) technique. ECG-gating is used to reduce cardiac pulsation artifacts. The b-SSFP pulse sequence is applied in mid- to end-diastole. (*C*) Depicts selected three slices from the final 3D-MRA volume, depicting pulmonary arteries, SVC, and aorta (top image), ventricular outflow tracts and left coronary origin (middle image), and four-chamber view and right and left coronary arteries in atrioventricular grooves (bottom image) with a high in-plane spatial resolution (1.3 mm × 1.3 mm).

thoracoabdominal and peripheral MRA, spatial saturation pulses are placed below the selected slice as the direction of venous flow in the extremities and inferior vena cava (IVC) is caudocranial. For thoracoabdominal and peripheral MRV, the spatial saturation pulses are placed above the selected slice to suppress arterial inflow.

For optimal TOF imaging, the flow needs to be fast and the slice needs to be thin, so that the blood within the selected saturated slice is entirely replaced by fast-inflowing unsaturated spins during acquisition, which produces the maximum signal. Thus this sequence works best when the blood flow velocity is greater than the slice

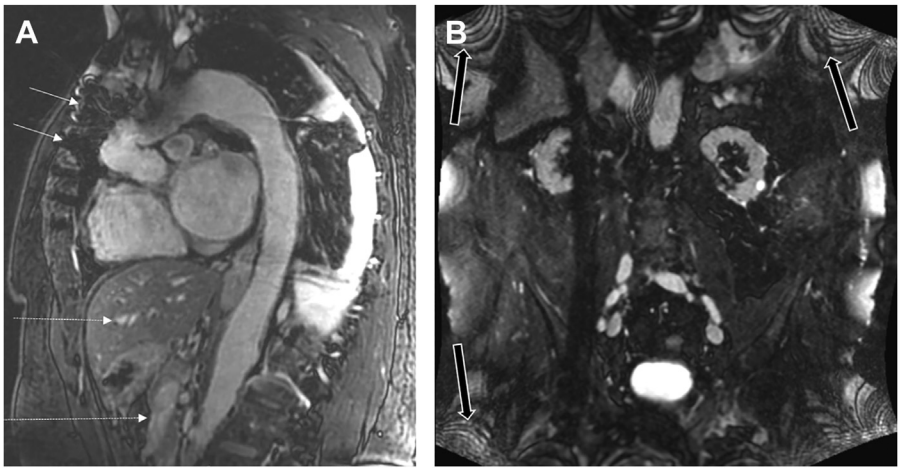

Fig. 3. Common pitfalls with b-SSFP MRA. Pitfalls include metallic susceptibility artifacts due to sternotomy wires (*solid white arrows*, *A*), simultaneous visualization of venous signal from portal vein, hepatic veins, and IVC (*dotted white arrows*, *B*) and Moire'/fringe artifacts at edges (*block arrow*, *B*).

Descargado para Anonymous User (n/a) en National Library of Health and Social Security de ClinicalKey.es por Elsevier en julio 13, 2023. Para uso personal exclusivamente. No se permiten otros usos sin autorización. Copyright ©2023. Elsevier Inc. Todos los derechos reservados.

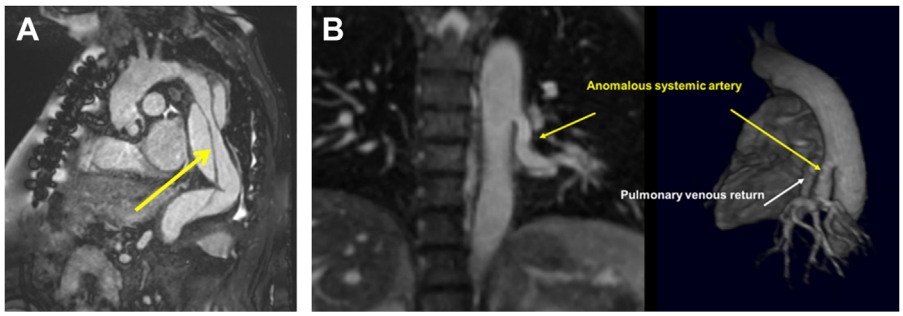

Fig. 4. Clinical applications of 3D-b-SSFP MRA. (*A*) Selected image from 3D acquisition shows aortic dissection in the thoracic aorta (*arrow, A*) (*B*) 3D-b-SSFP in a case of intralobar pulmonary sequestration demonstrated the anomalous systemic artery arising from the descending thoracic aorta and drainage into pulmonary vein.

thickness and TR.[12] Another requirement for optimal TOF imaging is that vessels need to be perpendicular to the selected slice. This can be a challenge for 3D-TOF where some of the moving spins are partially saturated through a 3D slab and lose optimal signal. This can be mitigated by the use of multiple overlapping thin slab acquisition technique and spatially variable (ramped) RF pulses, such as spins entering a slab experience less saturation (due to smaller flip angles) compared to spins exiting a slab (due to larger flip angles).[26–28] The use of magnetization transfer RF pulse allows for better background suppression and higher SNR.[28] As with any MRA technique, tradeoffs occur with parameter optimization. For example, longer TR increases vascular signal but also static tissue signal, and thus, TR is kept between 15 and 35 msec. Longer TE increases vascular signal but turbulent flow can also cause loss of signal due to flow dephasing and thus TE is kept between 3 and 7 msec. TOF is also commonly paired with flow-compensated gradient-echo readouts (eg, b-SSFP) to reduce signal loss from spin flow dephasing. Good contrast between static tissue and blood signal is provided when flip angles between 30° and 70° are used for 2D TOF and between 10° and 30° for 3D-TOF. For peripheral extremity MRA, ECG-gating is needed to avoid ghosting from multiphasic flow.[29]

Limitations

TOF is insensitive to in-plane flow, thus, the area imaged must be perpendicular to the image slice. Stenosis can be overestimated and artifacts can be produced by turbulent in-plane flow in segments with non-perpendicular anatomy (eg, at the carotid bulb and intracranial MRV) (Fig. 6). In the subclavian steal syndrome, the reversal of flow in the vertebral artery may be mistaken for occlusion when spatial saturation pulses are applied above the imaging slice. The correct diagnosis of vertebral artery flow reversal can be confirmed by repeating TOF with spatial saturation pulse applied below the slice or with the PC-MRA technique.[30]

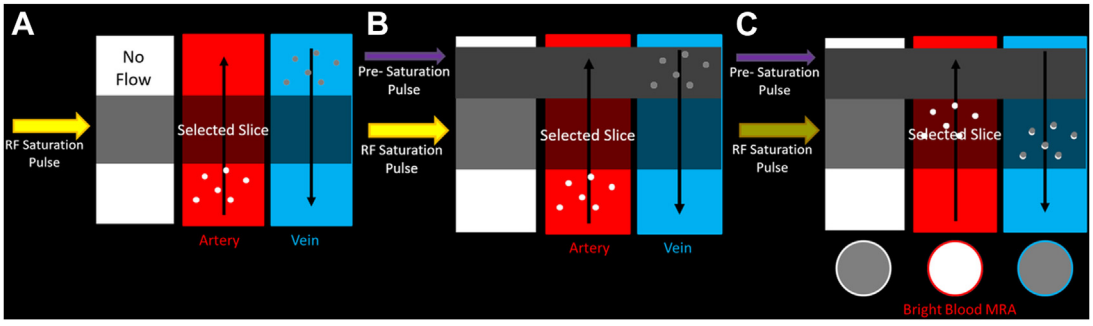

Fig. 5. Schematic of TOF-MRA as applied to head and neck region. The arteries have caudo-cranial flow and veins have cranio-caudal flow (*black arrows*). (*A*) Depicts application of initial multiple slice-selective RF pulses (*yellow block arrow*) to partially saturate background static signal. (*B*) Depicts application of spatial saturation pulse above the slice to be imaged (*purple arrow*) to suppress unwanted signal from the inflowing venous flow. (*C*) Depicts final MRA images at the time of readout such that inflowing unsaturated spins in the artery produce BB images while inflowing saturated signals in the vein appear dark.

Descargado para Anonymous User (n/a) en National Library of Health and Social Security de ClinicalKey.es por Elsevier en julio 13, 2023. Para uso personal exclusivamente. No se permiten otros usos sin autorización. Copyright ©2023. Elsevier Inc. Todos los derechos reservados.

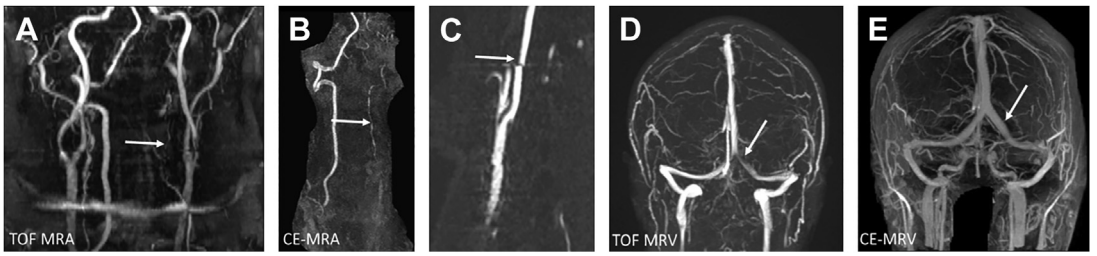

Fig. 6. Schematic and clinical applications of 3D-TOF-MRA in the brain. (*A*) Depicts acquisition of intracranial 3D-TOF-MRA with the selected region of interest and venous saturation pulse. (*B*) Maximum Intensity Projection (MIP) image from 3D-TOF-MRA shows a normal Circle of Willis anatomy. (*C*, *D*) Axial source (*C*) and MIP (*D*) images from 3D-TOF-MRA in a patient with a right parietal arteriovenous malformation show nidus (*white arrow*, C), prominent draining veins (*dashed arrow*, *C*), and arterial feeders from the middle cerebral artery (*white arrow*, *D*) and posterior cerebral artery (*dashed arrow*, *D*). (*E*) Axial image from 3D-TOF (*E*) in a patient with Moya-Moya disease well demonstrates bilateral lenticulostriate collaterals (*white arrows*, *E*) when compared with CE-MRA.

TOF is suboptimal for imaging renal and visceral arteries as these arise in an axial or oblique plane from the aorta. In patients with severe peripheral vascular disease, distal arteries with slow flow are poorly visualized. TOF images are also affected by respiratory motion in the abdomen and by swallowing motion in the neck. As 2D-TOF needs separate acquisition for each station, this can lead to stair step artifacts and long imaging times for peripheral vasculature (see **Fig. 6**). Compressed sensing, iterative reconstruction, and acceleration using parallel imaging techniques can be used to minimize scan times for single station at a time, and for 3D-TOF-MRA.[31–33]

Common Clinical Applications

Two-dimensional TOF-MRA is best suited for imaging fast arterial flow of the cervical and carotid vessels. TOF is less preferred than QISS for peripheral vasculature imaging due to the above-mentioned limitations for visualizing slow distal flow and overestimating stenosis. Three-dimensional TOF is best for intracranial MRA and has been widely used for the detection of aneurysms, stenosis, occlusions, arteriovenous malformations, and post-intervention imaging, where longer scan times are not a problem due to lack of motion in the brain (**Fig. 7**).[34,35] However, for MRV, the 3D-TOF technique is less preferred than PC-MRV (see below).

QUIESCENT INTERVAL SINGLE-SHOT

Principle

Similar to TOF, quiscent interval single-shot (QISS) is also based on the principle of inflow-dependent enhancement in perpendicularly oriented vessels. QISS is traditionally performed using ECG-gating and b-SSFP single-shot technique. In QISS acquisition, shortly after R-wave, a slice-selective pulse is applied along with the application of spatial saturation pulse above or below for arterial or venous flow suppression and followed by a fat suppression pulse. Following a quiescent interval of ~ 230 msec (range 200–300 msec) timed to systole, such that maximum systolic-inflow occurs into the selected slice, a b-SSFP readout gradient is applied and images are acquired at end-diastole (**Fig. 8**).[36]

QISS offers several advantages over TOF for peripheral vascular imaging. In QISS, as the QI is much longer than TR used in TOF, it allows a greater time for arterial inflow and is better suited for detecting residual flow in diseased peripheral segments with a slow flow (which can be overestimated on TOF as absent flow).[36] QISS is more rapidly acquired than TOF with a single-shot acquisition per slice. QISS can also be tailored for peripheral venous imaging by increasing the duration of the quiescent interval to allow more venous inflow and reversing the location of spatial saturation pulse.[37]

Limitations

Similar to TOF, QISS is sensitive to through-plane flow and is best suited for perpendicular vessels in the lower extremities. However, newer advances with QISS optimize the method for imaging the vasculature in other body regions too.[38] QISS is sensitive to inhomogeneity and susceptibility artifacts related to the b-SSFP readout. Using a fast low-angle shot readout can mitigate b-SSFP-related artifacts. However, tradeoffs include lower SNR and greater flow saturation.[39] Like all ECG-gated MRA sequences, QISS is suboptimal in patients with arrhythmias. To overcome this, Edelman, and colleagues and Koktzoglou and colleagues, have recently developed ungated-QISS (unQISS) and fast interrupted steady-state (FISS)-MRA.[40,41] Although both these "second-generation QISS"-MRA sequences do not require ECG-gating, due

Descargado para Anonymous User (n/a) en National Library of Health and Social Security de ClinicalKey.es por Elsevier en julio 13, 2023. Para uso personal exclusivamente. No se permiten otros usos sin autorización. Copyright ©2023. Elsevier Inc. Todos los derechos reservados.

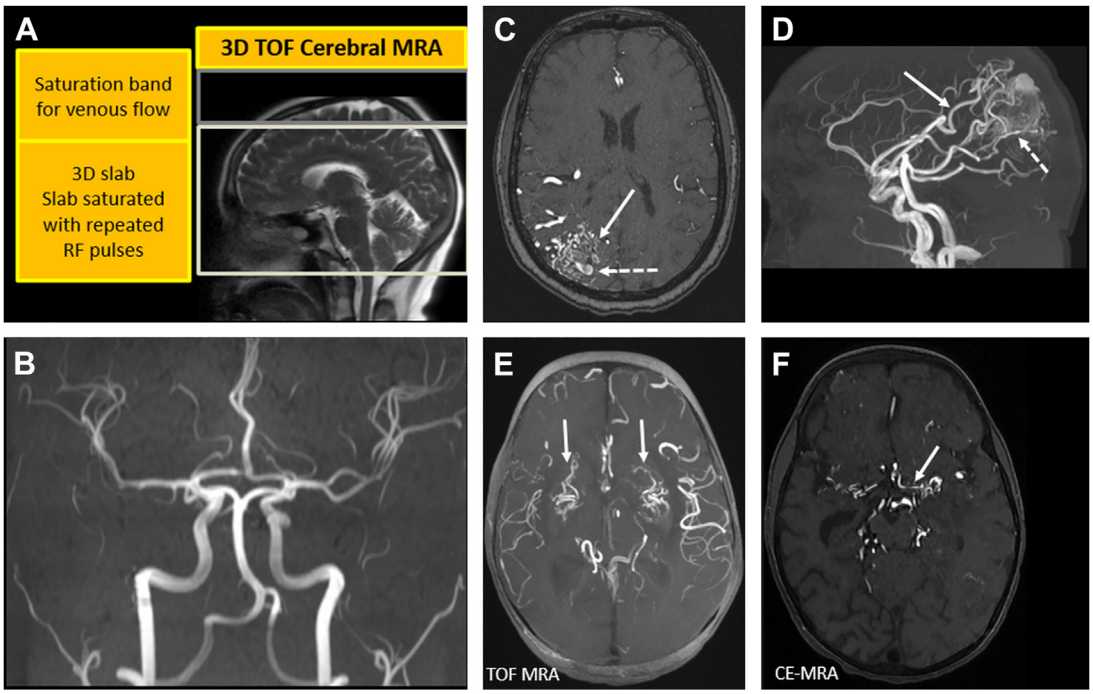

Fig. 7. Common pitfalls with TOF-MRA technique. (*A*, *B*) TOF-MRA overestimated left vertebral artery stenosis (*arrow*, *A*) compared to CE-MRA (*arrow*, *B*). This is due to turbulent flow causing loss of signal. (*C*) Swallowing and neck motion between slabs can lead to stair-steps artifacts (*arrow*) in the carotid MRA. (*D–F*) There is a partial loss of signal in left transverse venous sinus due to through-plane flow on TOF-MRV (*arrow*, *D*), corresponding CE-MRV shows widely patent left transverse sinus (*arrow*, *E*).

to longer scan times, these are better suited for imaging body regions unaffected by respiratory motion including the peripheral veins and extracranial carotid arteries.[38,42,43]

Common Clinical Applications

Since its initial description, QISS has been widely adopted for imaging peripheral arterial disease in lower extremities given the ease of acquisition and its high accuracy for detecting diseased segments when compared with CE-MRA or digital subtraction angiograms (DSA) in multiple studies (**Fig. 9**).[29,44,45] A meta-analysis including 17 studies demonstrated that QISS has a pooled sensitivity, specificity, and accuracy of 0.88 (95% CI: 0.85–0.91), 0.94 (95% CI: 0.92–0.96), and 0.96 (95% CI: 0.94–0.98), respectively, on a per-segment basis

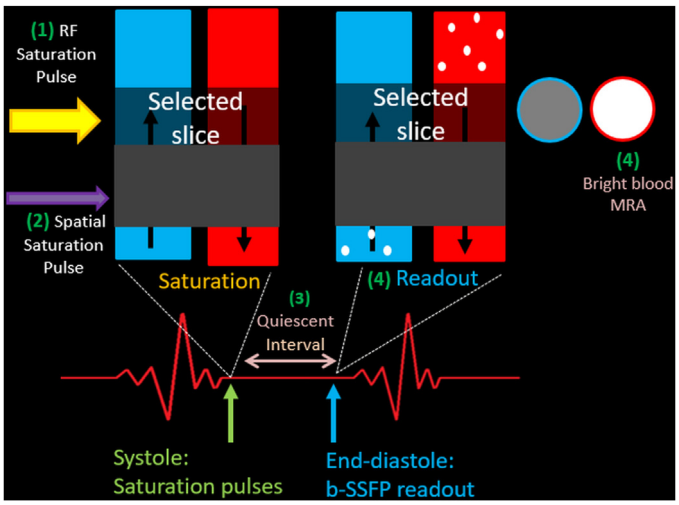

Fig. 8. Schematic of QISS sequence as applied to peripheral limb MRA. The direction of flow in the artery and vein is denoted by black arrows. The sequence is ECG-gated. (1) Shortly after R-wave in systole, slice-selective saturation pulse (*yellow block arrow*) is applied in the region of interest. (2) Application of spatial saturation pulses (*purple arrow*) above selected slice for suppression of venous signal and fat saturation pulses. (3) After a quiescent interval, fresh blood washes in the selected slice. (4) Single-shot b-SSFP readout is applied at end diastole for the final BB MRA images.

Descargado para Anonymous User (n/a) en National Library of Health and Social Security de ClinicalKey.es por Elsevier en julio 13, 2023. Para uso personal exclusivamente. No se permiten otros usos sin autorización. Copyright ©2023. Elsevier Inc. Todos los derechos reservados.

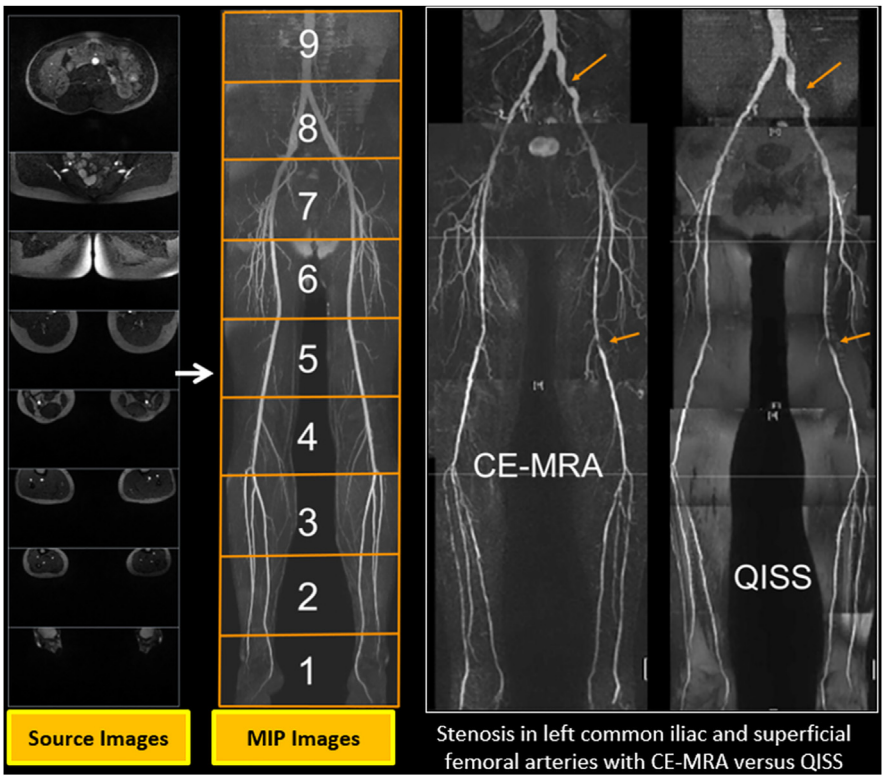

Fig. 9. Peripheral limb MRA with QISS denoting peripheral artery disease. The acquisition is a multi-station acquisition such that a series of 2D slabs are acquired from the abdomen to feet. The axial source images are used to generate MIP images per slab which are fused to create a peripheral run-off MRA. The final fused image derived from the QISS-MRA depicts short segment stenosis in the left common iliac artery (*top arrow*) and left superficial femoral artery (bottom *arrow*), which is concordant with the findings on CE-MRA. The total scan time for this QISS-MRA acquisition was ~12 minutes at 1.5 minutes/slab.

when compared with DSA/CE-MRA as reference for peripheral arterial disease.[44] QISS has also been used for upper extremity MRA with detailed visualization of distal arteries and palmar arches.[46]

Recently, QISS has been applied to patients undergoing pre-transcatheter aortic valve replacement (TAVR) workup in whom CT angiography is contraindicated due to impaired renal function.[47,48] QISS can be acquired along with a proton-density-weighted in-phase stack-of-stars pulse sequence that can simultaneously identify vascular calcifications comparable to CTA. Identification of vascular calcifications can be useful to guide the site of percutaneous arterial puncture during TAVR.[49]

QISS can be performed with breath-hold imaging or free breathing with navigator-respiratory gating for mesenteric, thoracic, and pulmonary MRA.[38,50,51] QISS can also be combined with non-Cartesian radial sampling for coronary and cerebrovascular imaging.[50,52–55] Radial QISS can also provide a non-contrast, radiation-free alternative to CTA for follow-up after endovascular aortic aneurysm repair (EVAR) procedures in the abdomen. In a head-to-head comparison between CTA and radial QISS, radial QISS had good image quality near the EVAR prosthesis and detected additional slow-flow type II endoleaks which were not seen on CTA.[56]

CARDIAC-GATED SUBTRACTIVE 3D-FAST SPIN-ECHO- MRA

Principle

Fast spin-echo (FSE) sequences are extremely sensitive to spin dephasing with fast-flowing blood producing a signal void. This flow-related sensitivity of FSE is harnessed for MRA by using ECG-gating to acquire two successive coronal oblique 3D slabs of images; one at peak systole and one at end diastole. During peak systole, arteries have the fastest flow, which produces flow voids or dark blood (DB) images. During end diastole, there is relatively slower flow in arteries compared to systole with some preservation of signal leading to BB images. Subtraction of systole (S) from diastole (D) images (D-S) demonstrates arterial flow as BB imaging.

Descargado para Anonymous User (n/a) en National Library of Health and Social Security de ClinicalKey.es por Elsevier en julio 13, 2023. Para uso personal exclusivamente. No se permiten otros usos sin autorización. Copyright ©2023. Elsevier Inc. Todos los derechos reservados.

The venous flow being slower than arterial flow appears bright on both systole and diastole and thus appears dark on the final (D-S) subtracted images (Fig. 10). Subtraction also suppresses background static tissue, which can be further suppressed by applying fat suppression techniques during readout. To enable fast imaging, a partial Fourier scheme, long-echo train length, and parallel imaging are used, along with ultra-short echo spacing to prevent complete spin dephasing for creation of BB images.[13,57] Unlike the previously described inflow-enhancement-based sequences, which require vessels to be perpendicular to the imaging slice, this sequence is less sensitive to the orientation partitions relative to vessels.

There are several factors that determine the visualization of vessels in this sequence, which are described in detail in the review by Wheaton, and colleagues.[12] Briefly larger arteries are better demonstrated by the use of higher refocusing flip angles (160° +) and the use of partial flow-compensating readout gradients. Conversely, smaller arteries are better visualized by the use of low refocusing flip angles (<120°) and the use of additional flow-dephasing gradients during readout.[12] An ECG-gated 3D-FSE with variable flip angles and flow-dephasing gradients has also been described for visualization of distal arteries in hands.[58] This sequence with 3D-FSE readout is also more immune to B0 inhomogeneity compared to QISS with b-SSFP readout and is better suited for large volumes of coverage and thoracoabdominal MRA.

Limitations

As an ECG-gated sequence, it is affected by cardiac arrhythmias. Due to its subtractive nature and acquisition of two scans over multiple R-R intervals, scan times are longer for extremity MRA. Even though both systolic and diastolic scans are acquired successively, artifacts due to patient motion and incomplete subtraction can still occur. This sequence also requires multiple ECG-prep scans at different trigger delays with manual selection of the correct ECG-trigger delays for systolic and diastolic images. Additionally, this sequence is not suitable for carotid MRA due to rapid flow in internal jugular veins which also shows similar flow-related dephasing effects. In cases of severe stenosis with increased turbulent flow, 3D-FSE-MRA can overestimate stenosis as even diastolic phase images now appear dark, and subtracted images show flow voids instead of the expected bright signals. Thus, it is necessary to review both subtracted images and diastolic images together to detect critical stenosis.[12,59]

Common Clinical Applications

Given its robustness to susceptibility effects, 3D-FSA-MRA can be used for the assessment of the thoracoabdominal aorta and pulmonary arteries with good visualization of pulmonary branches in the lungs and vessels adjacent to metallic devices. For imaging the thoraco-abdominal aorta, a single diastolic acquisition can suffice to produce BB MRA, as there is little venous contamination or background signal in this region (Fig. 11).[60] In pulmonary MRA, subtraction of systolic from diastole images also provides pulmonary perfusion MRA that can be used for detecting perfusion deficits associated with pulmonary embolisms.[61,62]

This sequence can be used for peripheral vascular MRA, but head-to-head comparisons showed a greater proportion of non-diagnostic

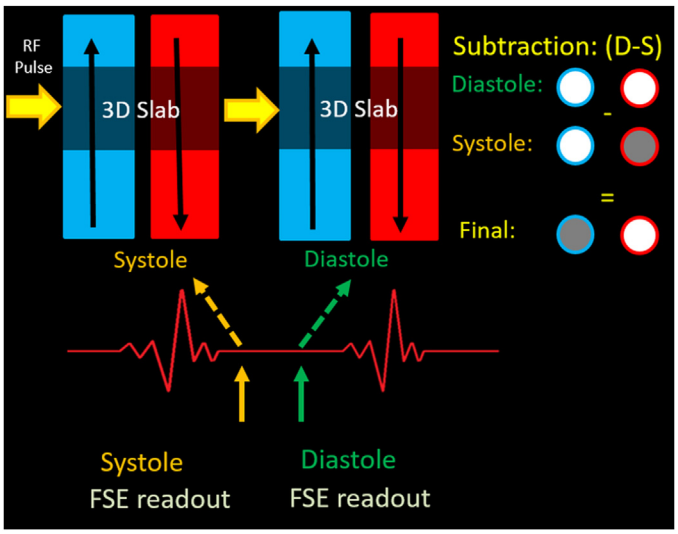

Fig. 10. Schematic for 3D-FSE-MRA technique as applied to peripheral limb MRA. The direction of flow in the artery and vein is denoted by black arrows. In this ECG-gated subtractive technique, RF pulses are applied to selected 3D slabs in both systole and diastole with FSE readout. In diastole, both artery and vein produce a bright signal, while in systole artery show a loss of signal due to fast flow-related dephasing while the vein is bright due to slow non-pulsatile flow. Subtraction of systole from diastole (D-S) produces final BB MRA images as venous flow is canceled and arterial flow is accentuated.

Descargado para Anonymous User (n/a) en National Library of Health and Social Security de ClinicalKey.es por Elsevier en julio 13, 2023. Para uso personal exclusivamente. No se permiten otros usos sin autorización. Copyright ©2023. Elsevier Inc. Todos los derechos reservados.

segments with ECG-gated 3D- FSE compared to QISS-MRA.[63] Sensitivities for 3D-FSE-MRA and QISS, were similar but ECG-gated 3D–FSE showed slightly lower specificity. 3D-FSE-MRA images of proximal pelvic and distal pedal arteries were limited compared to QISS, with greater susceptibility to patient motion.[64] However, given the high negative predictive value, 3D-FSA-MRA can be useful as a screening modality (see **Fig. 11**).[29,65] Other applications include non-contrast peripheral MR venography by additional subtraction of subtracted images from systole images [S-(D-S)] and non-contrast MR portography with good visualization of the intrahepatic and extrahepatic portal circulation.[66] Similar to aortic 3D-FSE-MRA, a single diastolic phase acquisition with an appropriately selected diastolic phase trigger delay depicts the portal circulation as BB while the background signal from the aorta is suppressed.

3D- BALANCED STEADY-STATE FREE-PRECESSION WITH FLOW-SENSITIVE DEPHASING

Principle

This is another ECG-gated subtractive technique based on the same principle of DB imaging during peak systole and BB imaging during end diastole. Instead of an FSE readout, flow-sensitive dephasing (FSD) gradients are applied along vessel length with a b-SSFP readout. This sequence uses an FSD pre-pulse along with large bipolar gradients to produce flow-related loss of signal from moving spins. The FSD pre-pulse comprises alternate +90°-x, +180°-y, −90°-x pulses and interleaved bipolar gradients on either side of +180°-y pulse. After excitation by the initial +90°-x pulse, spins are dephased by bipolar gradients depending on their velocities. With optimally selected bipolar gradients, a greater degree of spin dephasing occurs

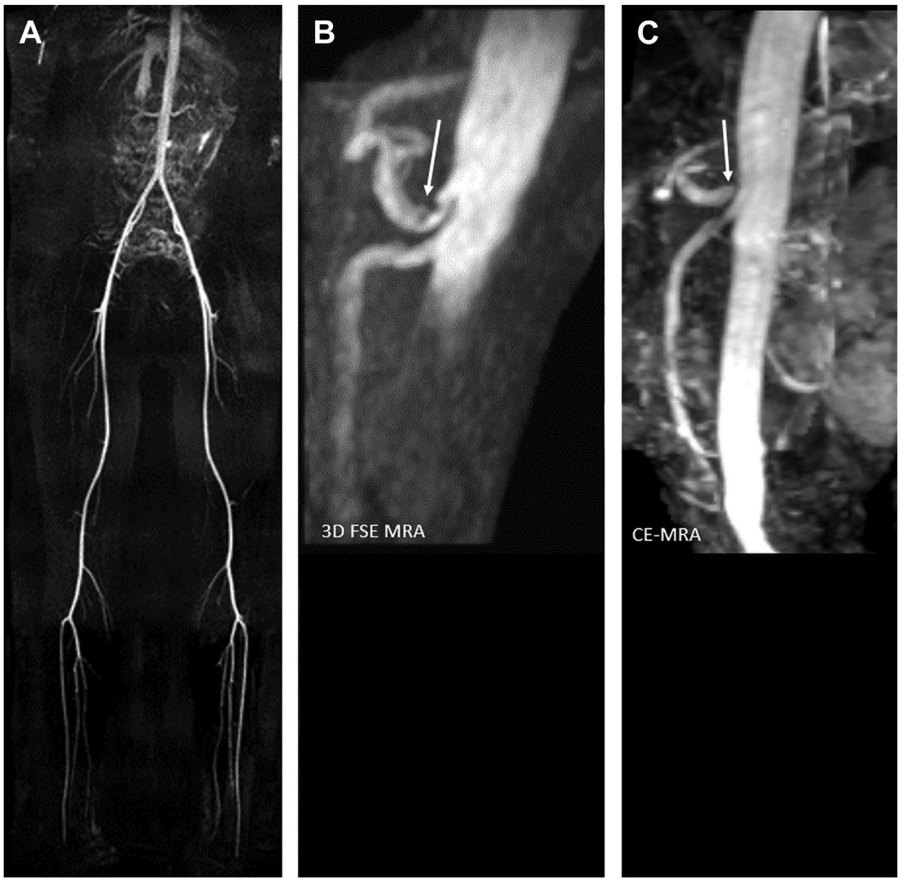

Fig. 11. Clinical applications of 3D-FSE-MRA. (*A*) Aorto-iliac and peripheral MRA with 3D-FSE-MRA in the patient shows a good depiction of all vessels thereby excluding atherosclerotic disease. (*B*, *C*) Median arcuate ligament syndrome. There is severe ostial stenosis of the celiac trunk with hook-like superior indention (*arrow*) seen on non-contrast 3D-FSE-MRA in a patient with post-prandial abdominal pain. This finding is also confirmed on a CE-MRA MRA suggestive of median arcuate ligament syndrome (*arrow*).

Descargado para Anonymous User (n/a) en National Library of Health and Social Security de ClinicalKey.es por Elsevier en julio 13, 2023. Para uso personal exclusivamente. No se permiten otros usos sin autorización. Copyright ©2023. Elsevier Inc. Todos los derechos reservados.

in arteries with little effect on veins or background signals. Following the application of bipolar gradients, the −90°-x flip back pulse restores longitudinal magnetization of rephased spins to produce a signal while a spoiler gradient prevents refocusing of dephased spins in later modules (**Fig. 12**). During systole, the FSD pre-pulse is applied with bipolar gradients turned on to produce DB images, while during diastole, the FSD pre-pulse is applied with all bipolar gradients turned off to produce BB images, followed by (D-S) subtraction to accentuate arterial flow and strongly suppress background flow.[67,68]

This sequence produces better DB images in systole compared to 3D-FSE. However, the technical success of this sequence and vessel visibility depends on the strength and duration of bipolar gradients. Large bipolar gradients increase flow-sensitivity and thus may lead to simultaneous visualization of veins as well as background tissue due to the diffusion effect. Smaller bipolar gradients decrease flow-sensitivity with impaired visualization of small arteries with lower velocities, and resultant overestimation of stenosis.[69] The FSD pre-pulses can also be applied in all three orthogonal planes to detect flow in multiple directions in hands and feet.[70]

Limitations

Other limitations are similar to those of ECG-gated subtracted techniques (eg, selection of appropriate triggers for systolic and diastolic images, sensitivity to cardiac arrhythmias, patient motion, and long scan times) and those of b-SSFP readout (eg, susceptibility to B0 inhomogeneity). Additionally, this sequence is not commercially available.

Current Clinical Applications

The initial studies showed utility for visualization of infragenual (below the knee) arteries, and small arteries of feet and hands in patients with diabetes and autoimmune vasculopathies (**Fig. 13**).[71–76]

PHASE-CONTRAST-MRA (3D AND 4D FLOW IMAGING)

Principle

This is based on the principle that moving spins experience a net shift in the phase when exposed to bipolar gradients, while stationary spins show no net-phase shift. The net shift in the phase is proportional to the velocity of moving spins, thus this is a velocity sensitive technique. In this sequence, three flow-encoding bipolar gradients with pre-determined velocity encoding (Venc) and one flow-compensated bipolar gradient are applied in three orthogonal directions to generate pairs of datasets. These pairs of datasets are subtracted from each other to produce phase (flow information) and magnitude (anatomic information) images. As stationary spins experience no net-phase shift, these are inherently suppressed on subtracted images. The Venc is decided by the

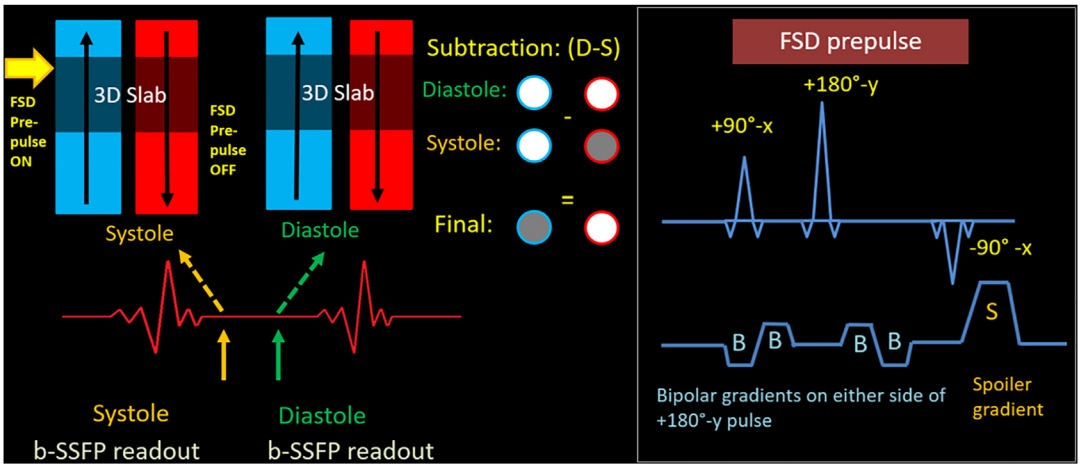

Fig. 12. 3D-b-SSFP FSD MRA technique as applied to peripheral limb MRA. The direction of flow in the artery and vein is denoted by black arrows. In this ECG-gated subtractive technique with b-SSFP readout, acquisition in systole is done with the FSD pre-pulse turned on. In diastole, the FSD pre-pulse is turned off. Both artery and vein produce a bright signal in diastole; the artery shows loss of signal due to FSD in systole. Subtraction of systole from diastole (D-S) produces final BB MRA images. The diagram on the right shows FSD pre-pulse comprising +90°-x, +180°-y, −90°-x pulses with interleaved bipolar gradients on either side of +180°-y pulse. Spoiler gradient applied after 90°-x pulse prevents refocusing of dephased spins in later modules. The sensitivity of this sequence to depict arterial flow depends on the strength and duration of these bipolar gradients.

Descargado para Anonymous User (n/a) en National Library of Health and Social Security de ClinicalKey.es por Elsevier en julio 13, 2023. Para uso personal exclusivamente. No se permiten otros usos sin autorización. Copyright ©2023. Elsevier Inc. Todos los derechos reservados.

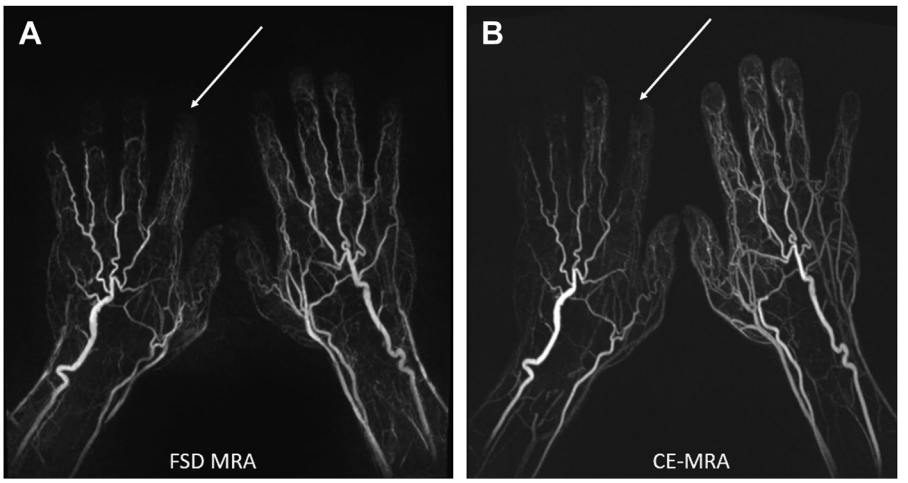

Fig. 13. Clinical application of 3D-b-SSFP FSD MRA in scleroderma. In this patient presenting with ischemia of the right hand index finger, 3D-FSD MRA demonstrates paucity of digital vessels at the tip of the right index finger (*arrow, A*), similar to CE-MRA (*arrow, B*). Also, note the attenuated distal vessels in other digits of the right hand seen on both non-contrast and CE-MRA images.

operator and is guided by the area of interest. The Venc should be set slightly higher than the maximum expected velocity at the time of scanning, such that at maximum velocities, the moving spins experience a net-phase shift of $\pm 180^{\circ}$ (**Fig. 14**). If the velocity of blood in the vessel of interest is greater than the pre-selected Venc, aliasing occurs leading to artifactual signal loss. If the Venc is much higher than the maximum velocity, then sensitivity for slow flow is decreased.[77] Typical settings for Venc are 150 to 200 cm/s in the thoracic aorta, 250 to 400 cm/s in the aorta with aortic stenosis or coarctation, 100 to 150 cm/s for intra-cardiac flow, and 50 to 80 cm/s in large vessels of the venous system.[78] To optimize SNR for non-contrast MRA of smaller vessels, a lower Venc can be used, such as 40 cm/second for non-contrast MRA of the renal arteries.[79] For MRA or MRV, a 3D or 4D acquisition is needed, a 2D acquisition may suffice for flow information (eg, for evaluation of valvular stenosis/regurgitation).[77,80]

In 4D-flow imaging, 3D phase-contrast (PC) imaging is used along with ECG-gating to produce time-resolved 3D cine flow across the cardiac cycle. Each 4D volume comprises one magnitude volume and three velocity/flow volumes in three spatial (x, y, z) directions (**Fig. 15**). Multiple display options are possible and additional quantitative analysis can be performed on dedicated post-processing software.[78,81] Due to the volumetric nature of acquisition, specific planning is not required, and any vessel can be evaluated in the included field of view. The technical details of 4D-flow are beyond the scope of this review, and have been described in other comprehensive reviews.[82,83]

Limitations

The scan time of PC-MRA depends on the specific sequence used and could be long. Some of the commercially available sequences could be performed more rapidly than the 3D-SSDP

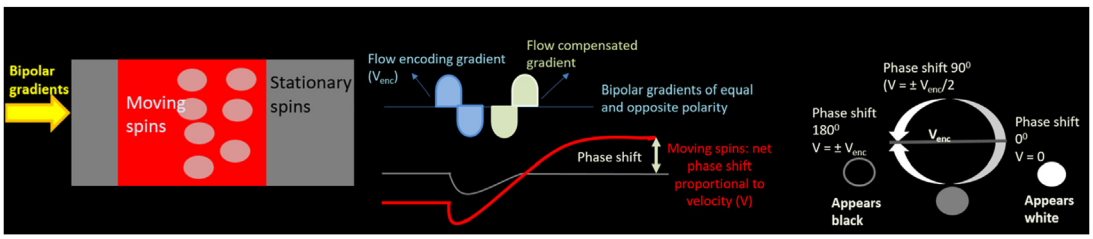

Fig. 14. Schematic for PC MRA. Bipolar flow-encoding gradients with pre-determined velocity (Venc) and flow-compensated gradient are applied in three orthogonal directions to produce pairs of images which are subtracted to produce BB images. The net-phase shift ranges from 00 to 1800, depending on the velocity (V) in relation to Venc. Stationary spins (V = 0) experience no phase shift and appear white. Moving spins (V $\leq$ Venc) show phase shift of up to 1800. Spins with V > Venc show aliasing as these experience phase shift greater than 1800.

Descargado para Anonymous User (n/a) en National Library of Health and Social Security de ClinicalKey.es por Elsevier en julio 13, 2023. Para uso personal exclusivamente. No se permiten otros usos sin autorización. Copyright ©2023. Elsevier Inc. Todos los derechos reservados.

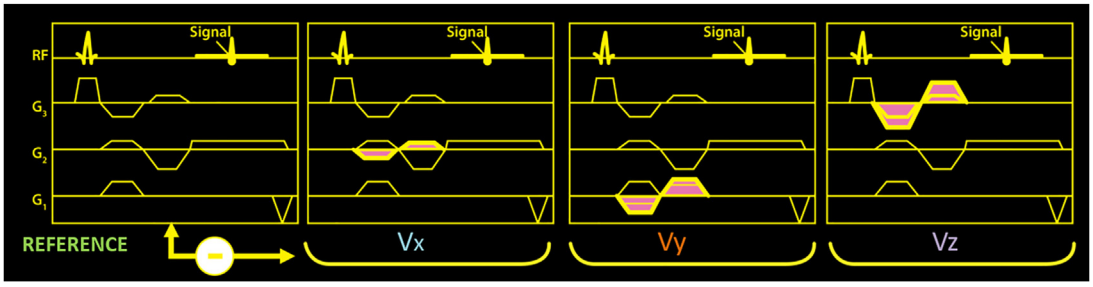

Fig. 15. 4D flow MR imaging. 4D flow MR acquisition comprises 3D PC imaging in three directions (x,y,x) using ECG-gating to provide time-resolved flow information across the cardiac cycle. Each 4D volume is comprised of one reference magnitude volume and three velocity/flow volumes in three spatial (Vx,Vy,Vz) directions.

sequence. 3D-PC-MRA is also prone to signal losses of turbulence and tortuosity. Parallel imaging, radial sampling, and compressed sensing have all been used to decrease scan times of 4D-flow imaging by a factor of four to six times, with preserved anatomic resolution and accurate flow quantification.[84,85]

Current Clinical Applications

Clinically, 3D-PC-MRA has been limited to the evaluation of mesenteric and native and transplant renal arteries. For renal artery imaging, significant flow-dephasing and signal loss in areas of turbulence indicates hemodynamically significant stenosis.[86] In the brain, 3D-PC-MRA can be used as an alternative to 3D-TOF-MRA in the presence of hemorrhage or subacute thrombosis to avoid diagnostic pitfalls induced by artifactual T1 shine-through effect on TOF-MRA. In the brain, 3D-PC-MR venogram remains popular for the detection of cerebral venous sinus stenosis or thrombosis. A low-resolution PC-MRA is also commonly used as a scout image for identifying carotid arteries (**Fig. 16**).[13]

Multiple novel clinical applications of 4D flow imaging have been described in dedicated reviews.[78,83,87] The most common application of 4D-flow imaging lies in cardiovascular imaging to depict blood flow patterns in complex congenital cardiac diseases and aortopathies.[88,89] 4D-flow imaging is also being applied for abdominal imaging for evaluation of portal circulation as well as the abdominal aorta and its major branches (**Fig. 17**).[90] In, neurovascular imaging, 4D flow imaging can be useful for the evaluation of complex arteriovenous malformations and fistulas, intracranial aneurysms, and Moya-Moya disease.[87]

VELOCITY SELECTIVE MRA

Principle

In this technique, a velocity selective magnetization preparation pulse is applied at peak systole using ECG-gating which sensitizes the sequence to arterial flow while suppressing background stationary and venous flow. The velocity selective preparation pulse comprises multiple RF pulses of small flip angles, with interleaved repeated bipolar gradients.[91,92] This is usually combined

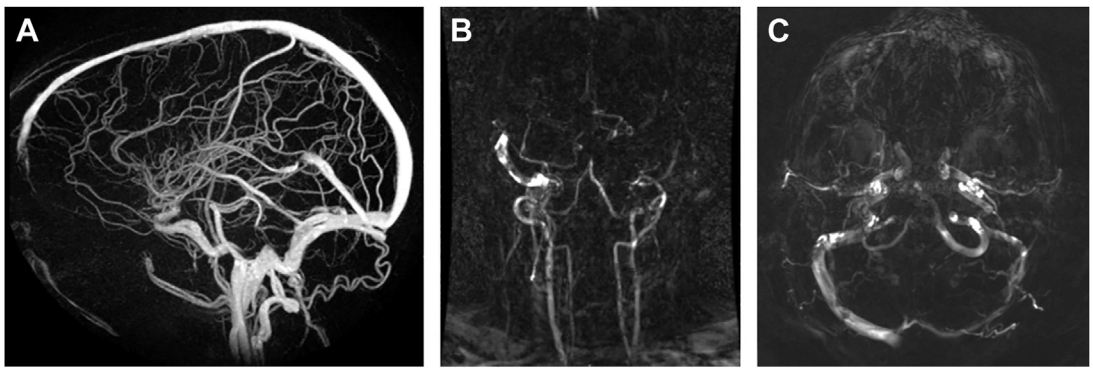

Fig. 16. Clinical applications of PC technique. (*A*) Example of 3D-phase-contrast cerebral MR venogram (MRV) showing excellent visualization of the patent cerebral venous sinuses. (*B*, *C*) Phase-contrast technique can also be used for scout images before TOF-MRA (*B*) and TOF-MRV (*C*).

Descargado para Anonymous User (n/a) en National Library of Health and Social Security de ClinicalKey.es por Elsevier en julio 13, 2023. Para uso personal exclusivamente. No se permiten otros usos sin autorización. Copyright ©2023. Elsevier Inc. Todos los derechos reservados.

Fig. 17. Clinical application of 4D flow MRA. MIP (*A*) and volume rendered (*B*) reconstructions from non-contrast PC-MR angiographic images from a 4D flow acquisition. This provides good anatomical information on renal vessel arteries (*arrow*) without the need for intravenous contrast, which is beneficial in patients with severe renal dysfunction or contrast allergies.

with b-SSFP readout, although alternatively gradient-echo readout can also be used to reduce the banding artifacts associated with b-SSFP (Fig. 18).

As the sequence is only applied in systole and diastolic acquisition is not needed, it is faster than the previously described ECG-gated subtractive MRA techniques and is insensitive to motion and cardiac arrhythmias. The sequence also has high spatial resolution and large coverage when used with 3D-b-SSFP readout.

Limitations and Current Clinical Applications

This sequence is not available commercially, however, it has been shown to be feasible for cerebral

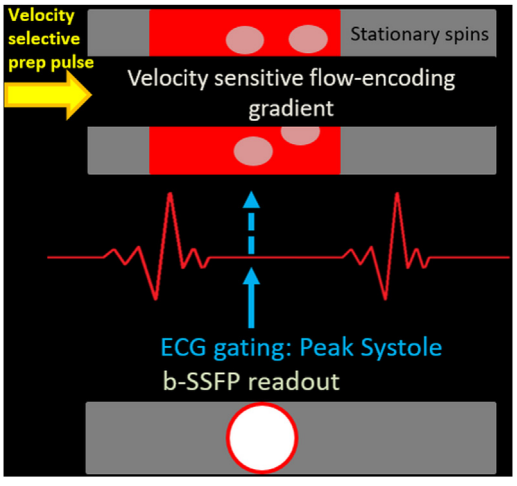

Fig. 18. Schematic for velocity selective MRA. In this ECG-gated sequence, a velocity selective preparation pulse that sensitizes to arterial flow and suppresses background stationary and venous flow is applied in peak systole with readout to produce BB images. No diastolic acquisition is performed.

MRA, abdominal MRA, and peripheral artery MRA.[93–95] The main clinical application lies in the evaluation of peripheral arterial disease in patients without stents or prostheses and with known cardiac disease.[95]

ARTERIAL SPIN LABELING MRA

Principle

Arterial spin labeling (ASL)-MRA techniques can be of three types: flow-in, flow-out, or alternate tag on-off/subtracted ASL-MRA. This sequence is based on the principle of selectively "tagging" the longitudinal magnetization of flowing blood using a selective inversion recovery pulse, such that a difference is created in the longitudinal magnetization between flowing blood and stationary tissue. Following tagging and an appropriately selected inversion time (TI) such that background tissue reaches the null point, blood flowing into (flow-in) or flowing out of (flow-out) of the tagged slab can be read out by either half-Fourier FSE or b-SSFP sequence with or without additional fat suppression sequences (Fig. 19).[13] In the "alternate tag on-off sequence", two alternate datasets are acquired with "tag on" and "tag off" which are subtracted from each other to generate BB images from the tagged region. Thus, in the "alternate tag on-off technique", background suppression relies on subtraction and is independent of the selected TI (see Fig. 19).[96] Between the two readout options, b-SSFP readout provides better resolution and the flow-compensated nature of b-SSFP sequence makes it preferable for most regions, except for distal pulmonary and subclavian vessels near air–tissue interfaces where half-Fourier FSE is preferred. Half-Fourier FSE readout may be suitable for imaging vessels with slow flow like hepatic veins, portal veins, and small vessels

Descargado para Anonymous User (n/a) en National Library of Health and Social Security de ClinicalKey.es por Elsevier en julio 13, 2023. Para uso personal exclusivamente. No se permiten otros usos sin autorización. Copyright ©2023. Elsevier Inc. Todos los derechos reservados.

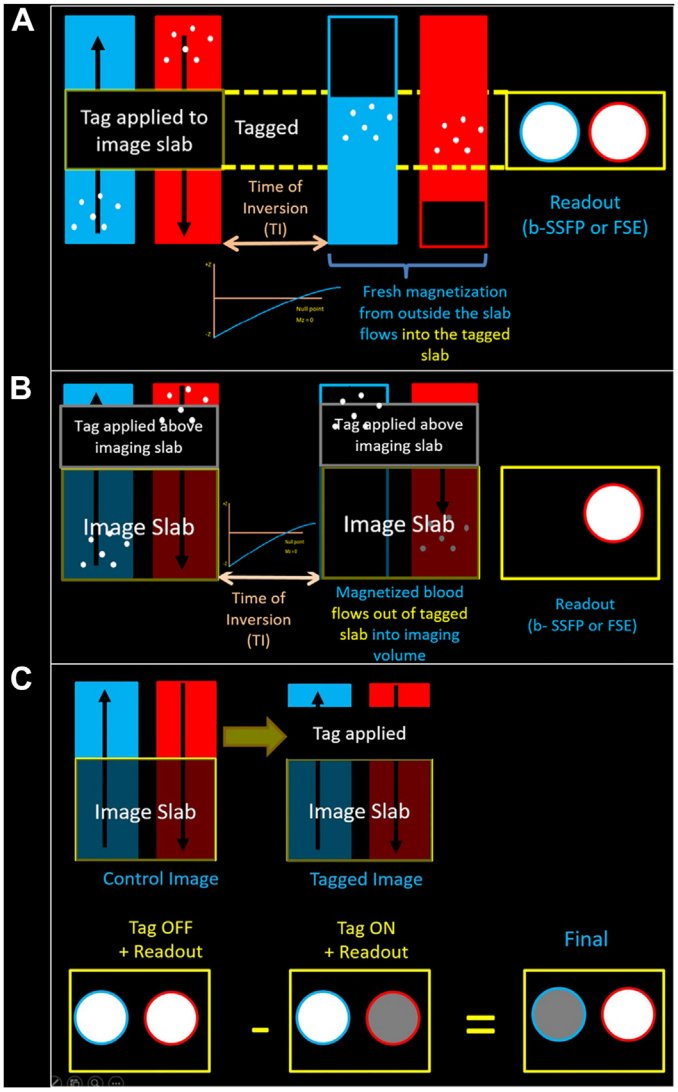

Fig. 19. Schematic for ASL-MRA techniques. (*A*) Flow-in ASL-MRA: Tag pulse applied to the entire image slab inverting both flowing spins (blood) and stationary spins in the slab. At the time of inversion (TI), spins in the imaging slab reach a null point and fresh inflowing blood with fully preserved longitudinal magnetization produces a bright signal at the readout. (*B*) Flow-out ASL-MRA: Initially, a non-selective inversion pulse is applied everywhere inverting both flowing spins (blood) and stationary spins in the slab. A selective tag pulse is applied on the vessel of interest upstream of imaging volume, thereby, restoring magnetization of tagged blood. At TI, stationary spins in the image slab reach a null point and the original blood in the image slab flows out. The freshly tagged blood upstream of image slab flows out of the tagged slab into the imaging volume and produces a bright signal at the readout. (*C*) Tag On/Off Subtractive ASL-MRA: In this subtractive technique, first a "tag on" image is acquired with tagging of arterial blood followed by the acquisition of a control "tag off" image. Subtraction removes stationary signal and only tagged spins produce BB images.

of hands and feet where the flow-related spin dephasing effect associated with FSE sequences is not so pronounced.[13]

Flow-in arterial spin labeling -magnetic resonance angiography: considerations and clinical applications

In this sequence, tagging is applied to the entire imaging slab such that both moving spins in blood and stationary spins in the background are inverted. After a certain TI, such that all spins (moving and stationary) in the tagged slab are at a null point, untagged blood flowing into the tagged slab with preserved longitudinal magnetization produces BB images.[13] Thus, in this sequence, the tagged slab overlaps with the imaging volume of interest (see **Fig. 19**). As all untagged blood flowing into the slab can produce a signal, individual contributions cannot be determined, such as superior mesenteric vein and splenic vein for portal circulation.[13] As venous flow can also be seen, an additional presaturation slab is needed.

This technique is most widely validated for renal MRA for the detection of renal artery stenosis in both native and transplant kidneys (**Fig. 20**). For renal artery imaging, the sequence can be done with breath-hold or with navigator-gated respiratory gating. A thick axial band of RF pulses is applied in the region of renal vessels to invert background tissue. Following a long waiting interval (typical T1: 1200–1800 msec at 1.5 T), the readout is performed with 3D-b-SSFP sequence (see **Fig. 19**). Just before the readout, fat suppression is applied. Imaging is typically done in the

Descargado para Anonymous User (n/a) en National Library of Health and Social Security de ClinicalKey.es por Elsevier en julio 13, 2023. Para uso personal exclusivamente. No se permiten otros usos sin autorización. Copyright ©2023. Elsevier Inc. Todos los derechos reservados.

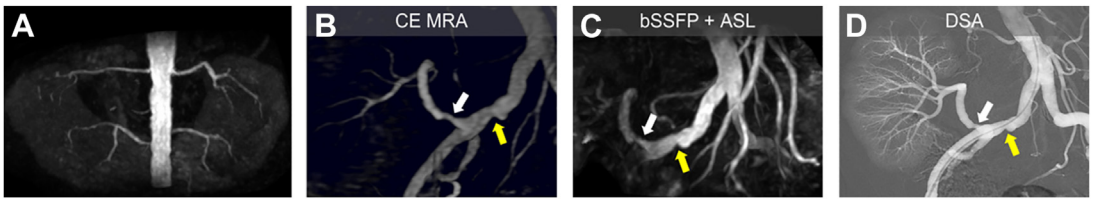

Fig. 20. Application of ASL-MRA in renal imaging. (*A*) ASL-MRA in a patient with a horseshoe kidneys and renovascular hypertension shows two renal arteries on each side without stenosis. (*B–D*) ASL-MRA in a patient with suspected transplant renal artery stenosis. Both CE-MRA (*B*) and ASL-MRA (*C*) show stenosis in the right common artery (*proximal yellow arrow*) and at the origin of the transplant renal artery (*white arrow*). These findings were confirmed on DSA (*D*). The gradient across the right common artery was greater than 10 mm Hg and angioplasty was performed. The gradient across the transplant renal artery was less than 10 mm Hg and no treatment was needed.

axial plane for maximum inflow effect and greater signal in arteries, but this is at the expense of decreased coverage for missing accessory renal arteries. The coronal plane can cover the entire abdomen to see accessory renal arteries, but there is signal loss inferiorly in the slab. This technique has shown high accuracy for the detection of renal artery stenosis in comparison with CTA, CE-MRA, or DSA.[97–102] In a multicenter study, ASL-MRA had sensitivity of 74%, specificity of 93%, and accuracy of 90% for the detection of stenosis in comparison with CTA.[100] In a study by Parienty and colleagues, the sensitivity, specificity, and accuracy of ASL-MRA were 93%, 88%, and 91%, respectively, for the diagnosis of a stenosis of 50% or greater when compared with DSA.[101,103] In a head-to head comparison between NC-MRA and CE-MRA, both techniques showed similar detection rates for diagnosis of renal artery stenosis but NC-MRA achieved better technical success rates, feasibility, and image quality in motion artifacts than CE-MRA.[102]

Flow-out arterial spin labeling -magnetic resonance angiography: considerations and clinical applications

In this sequence, first a non-selective inversion pulse is applied in the desired imaging volume to invert all magnetization (moving as well as stationary spins). This is followed by a selective inversion recovery pulse immediately upstream of the volume of interest which restores longitudinal magnetization of upstream tagged blood. At TI, stationary tissue in the imaging volume reaches the null point and the original blood in the imaging volume flows out. The tagged blood with fully restored longitudinal magnetization flows out of the tagged slab into the imaging volume to produce BB images.[13] In contrast to the flow-in technique, it is possible to select vessels with the flow-out technique as only vessels with tagged blood upstream of imaging volume will produce BB images (see **Fig. 19**).

This technique can be used for hepatic arteries, hepatic veins, and portal veins.[104–107] Double-tag techniques are used for hepatic veins with one inversion pulse (tag) on the upper liver to suppress inflowing blood from the aorta and another inversion pulse below the liver to suppress inflowing blood from portal veins.[105] Similarly for portal venograms, one inversion pulse is applied over the liver and thorax to suppress the liver, myocardium, and inflowing blood from hepatic arteries, and another inversion pulse is applied below the liver to suppress the inflowing blood from IVC.[107] Multiple tagged segments can also be used for acquisitions over a larger area of coverage for abdominopelvic MRA.[108] This technique has also been used for selective visualization of the external carotid artery and its branches.[109], and for separate visualization of pulmonary arteries and pulmonary veins by selectively placing an inversion pulse on the aorta and heart.[110]

Alternate tag on-off arterial spin labeling-magnetic resonance angiography: considerations and clinical applications

As this technique relies on subtractive effects between two datasets acquired with “tag on” and “tag off” (control), this is less reliant on the precise timing of TI. Unlike flow-in and flow-out ASL, where TI needs to be carefully selected to suppress background tissue, subtraction in alternate tag on-off ASL provides excellent background suppression. However, this is slower as at least two separate scans are required for subtraction. Multiple TIs can also be selected in an incremental manner for successive acquisitions to provide time-resolved MRA (or 4D-MRA). In time-resolved ASL-MRA too, the scan time increases proportionately to the number of TI increments.[12] However, with recent advances in MRI technology, 4D-MRA can capture dynamic information with comparable temporal and spatial resolution than dynamic CE-MRA and DSA.[111]

Descargado para Anonymous User (n/a) en National Library of Health and Social Security de ClinicalKey.es por Elsevier en julio 13, 2023. Para uso personal exclusivamente. No se permiten otros usos sin autorización. Copyright ©2023. Elsevier Inc. Todos los derechos reservados.

Table 2
Summary of non-contrast bright blood MRA techniques

	TOF	QISS	3D-B-SSFP	3D-FSE	3D-FSD	Phase- Contrast	VS-MRA	ASL-MRA
Gating	ECG-gating for peripheral MRA	ECG-gating	ECG-gating needed for cardiac, thorax, abdomen Breath-hold or respiratory gated	ECG-gating	ECG-gating	ECG-gating for 4D flow MRA	ECG-gating	Breath-hold or respiratory gated for thorax, abdomen
Subtraction required	No	No	No	Yes	Yes	No	No	For alternate tag technique
Preferred vasculature	Brain, carotid, less preferred for peripheral MRA	Lower extremity Newer QISS techniques: Additional regions	Coronary, aorta, great vessels of thorax, renal MRA	Large vessels of thorax, abdomen, pelvis Less preferred for extremities	Distal extremities, hands, and feet	Cardiac, renal, abdomen, brain 4D PC: Any vessel can be imaged	Lower extremity. Also feasible for cerebral MRA	Brain, carotid, renal, hepatic, portal, pulmonary
Vendor names Siemens	TOF	QISS	TrueFISP	NATIVE SPACE	Not commercially available	PC	Not commercially available	ASL-MRA
GE	TOF	-	FIESTA	Inhance Deltaflow		PC, Inhance Velocity		Inhance Inflow/ IFDIR
Philips	TOF	-	Balanced FFE	TRANCE		PC, Q-Flow		4D-TRANCE
Toshiba	TOF	-	True SSFP/FFE 3D	Fresh Blood Imaging		PS		mASTAR
Hitachi	TOF	VASC	Balanced SARGE	VASC-FSE		PC		VASL-ASL

Abbreviations: 3D: three-dimensional; ASL: arterial spin labeling; b-SSFP: balanced steady-state free precession; ECG: electrocardiogram; FSD: flow-sensitive dephasing; FSE: fast spin-echo; MRA: magnetic resonance angiography; QISS: Quiescent Interval Slice-Selective (QISS); TOF: time-of-flight ; VS: velocity selective.

Descargado para Anonymous User (n/a) en National Library of Health and Social Security de ClinicalKey.es por Elsevier en julio 13, 2023. Para uso personal exclusivamente. No se permiten otros usos sin autorización. Copyright ©2023. Elsevier Inc. Todos los derechos reservados.

This technique is most widely used for carotid and intracranial MRA.[112] Time-resolved ASL/4D-MRA can act as a radiation-free alternative to DSA for non-invasive alternative to DSA dynamic assessment of arteriovenous malformations or arteriovenous fistula in the brain.[113–115] In the brain, ASL with pseudo-continuous labeling can be modified to provide simultaneous MRA and perfusion information.[116] This technique can also be used for imaging of vascular malformations in the pelvis and peripheral extremities, pulmonary arteries in patients with chronic pulmonary thromboembolic disease, and regions with slower flow, for example, in pedal and digital arteries of the foot.[13,117]

MULTI-CONTRAST TECHNIQUES

Several groups of investigators have proposed multi-contrast techniques for simultaneous depiction of the vascular or cardiac chamber lumen with BB as well as the vessel and cardiac walls using DB contrast. The two most widely used techniques are Simultaneous Non-Contrast Angiography and Intra-Plaque Hemorrhage (SNAP), primarily used for carotid and cerebrovascular imaging[118] and inversion recovery prepared Magnetization Transfer Contrast Bright blOOD phase SensiTive (MTC-BOOST) that simultaneously generates co-registered 3D-BB and black-blood whole-heart images, which has been applied to the anatomical assessment of the pulmonary veins and left atrium as well in patients with congenital heart disease.[119]

Simultaneous Non-Contrast Angiography and Intra-Plaque Hemorrhage

The SNAP technique was developed for the assessment and characterization of carotid atherosclerosis and utilizes a phase-sensitive reconstruction that generates images with a negative signal corresponding to MRA and a positive signal corresponding to intra-plaque hemorrhage (IPH). By displaying only the negative signals, a non-contrast MRA is rendered with no contamination from background tissues. Alternatively, displaying only the positive signals yields a highly T1-weighted image suitable for IPH detection.[118] Several proof-of-concept studies have demonstrated the clinical feasibility of the SNAP technique with high accuracy for carotid stenosis grading as well as for the detection of carotid IPH.[120,121]

Magnetization Transfer -BOOST

The underlying principle of MTC-BOOST is a magnetization transfer prepared BB and black-blood phase-sensitive inversion recovery (PSIR) acquisition with two differently weighted BB volumes in an interleaved fashion. The two data sets are then combined in a PSIR-like reconstruction to obtain a complementary black-blood volume which can be used for visualization of the vessel wall or cardiac chamber walls. Image-based navigation and non-rigid respiratory motion correction are exploited for 100% scan efficiency and predictable acquisition time.[119]

Although both SNAP and MTC-BOOST can be considered investigational techniques, their dual contrast mechanism approach within a single acquisition generates high spatial resolution images with nearly perfect co-registration.

SUMMARY

There are multiple options for non-contrast MR angiography as described in this review. **Table 2** provides a summary of the available techniques, preferred clinical applications, and various vendor-specific trade names. Understanding the principles and the relative advantages and limitations of various non-contrast MRA techniques can enable appropriate sequence selection in various clinical scenarios where contrast administration is not preferred or contraindicated.

CLINICS CARE POINTS

- Balanced SSFP MRA is widely used for cardiothoracic, pulmonary, coronary, and abdominal MRA, providing background anatomical information.
- QISS is widely used in the evaluation of lower extremity arteries due to its ease of acquisition and high diagnostic accuracy.
- 3D-PC-MRA is used in the evaluation of mesenteric and native and transplant renal arteries.
- 4D-flow PC-MRA is commonly used to depict flow patterns in complex congenital heart disease and aortopathies.

DISCLOSURE

Dr P.S. Rajiah—Royalties from Elsevier.

REFERENCES

1. Schieda N, Maralani PJ, Hurrell C, et al. Updated Clinical Practice Guideline on Use of Gadolinium-Based Contrast Agents in Kidney Disease Issued by the Canadian Association of Radiologists. Can Assoc Radiol J 2019;70(3):226–32.

Descargado para Anonymous User (n/a) en National Library of Health and Social Security de ClinicalKey.es por Elsevier en julio 13, 2023. Para uso personal exclusivamente. No se permiten otros usos sin autorización. Copyright ©2023. Elsevier Inc. Todos los derechos reservados.

2. Gallo-Bernal S, Patino-Jaramillo N, Calixto CA, et al. Nephrogenic Systemic Fibrosis in Patients with Chronic Kidney Disease after the Use of Gadolinium-Based Contrast Agents: A Review for the Cardiovascular Imager. Diagnostics 2022; 12(8):1816.
3. Mathur M, Jones JR, Weinreb JC. Gadolinium Deposition and Nephrogenic Systemic Fibrosis: A Radiologist's Primer. Radiographics 2020;40(1): 153–62.
4. Runge VM. Critical Questions Regarding Gadolinium Deposition in the Brain and Body After Injections of the Gadolinium-Based Contrast Agents, Safety, and Clinical Recommendations in Consideration of the EMA's Pharmacovigilance and Risk Assessment Committee Recommendation for Suspension of the Marketing Authorizations for 4 Linear Agents. Invest Radiol 2017;52(6):317–23.
5. Murata N, Murata K, Gonzalez-Cuyar LF, et al. Gadolinium tissue deposition in brain and bone. Magn Reson Imaging 2016;34(10):1359–65.
6. McDonald JS, McDonald RJ. MR Imaging Safety Considerations of Gadolinium-Based Contrast Agents: Gadolinium Retention and Nephrogenic Systemic Fibrosis. Magn Reson Imaging Clin N Am 2020;28(4):497–507.
7. Jalili MH, Yu T, Hassani C, et al. Contrast-enhanced MR Angiography without Gadolinium-based Contrast Material: Clinical Applications Using Ferumoxytol. Radiol Cardiothorac Imaging 2022;4(4):e210323.
8. Available at: contrast_media.pdf. https://www.acr.org/-/media/acr/files/clinical-resources/contrast_media.pdf. Accessed February 27, 2023.
9. Edelman RR, Koktzoglou I. Non-contrast MR angiography: An update. J Magn Reson Imaging 2019; 49(2):355–73.
10. Kato Y, Ambale-Venkatesh B, Kassai Y, et al. Non-contrast coronary magnetic resonance angiography: current frontiers and future horizons. Magma N Y N 2020;33(5):591–612.
11. Navot B, Hecht EM, Lim RP, et al. MR Angiography Series: Fundamentals of Non–Contrast-enhanced MR Angiography. Radiographics 2021. https://doi.org/10.1148/rg.2021210141.
12. Wheaton AJ, Miyazaki M. Non-contrast enhanced MR angiography: Physical principles. J Magn Reson Imaging 2012;36(2):286–304.
13. Miyazaki M, Akahane M. Non-contrast enhanced MR angiography: Established techniques. J Magn Reson Imaging 2012;35(1):1–19.
14. Ludwig DR, Shetty AS, Broncano J, et al. Magnetic Resonance Angiography of the Thoracic Vasculature: Technique and Applications. J Magn Reson Imaging 2020;52(2):325–47.
15. Kourtidou S, Jones MR, Moore RA, et al. mDixon ECG-gated 3-dimensional cardiovascular magnetic resonance angiography in patients with congenital cardiovascular disease. J Cardiovasc Magn Reson 2019;21(1):52.
16. Heerfordt J, Stuber M, Maillot A, et al. A quantitative comparison between a navigated Cartesian and a self-navigated radial protocol from clinical studies for free-breathing 3D whole-heart bSSFP coronary MRA. Magn Reson Med 2020;84(1):157–69.
17. Fotaki A, Munoz C, Emanuel Y, et al. Efficient non-contrast enhanced 3D Cartesian cardiovascular magnetic resonance angiography of the thoracic aorta in 3 min. J Cardiovasc Magn Reson 2022; 24(1):5.
18. François CJ, Tuite D, Deshpande V, et al. Pulmonary vein imaging with unenhanced three-dimensional balanced steady-state free precession MR angiography: initial clinical evaluation. Radiology 2009;250(3):932–9.
19. François CJ, Tuite D, Deshpande V, et al. Unenhanced MR Angiography of the Thoracic Aorta: Initial Clinical Evaluation. Am J Roentgenol 2008; 190(4):902–6.
20. Potthast S, Mitsumori L, Stanescu LA, et al. Measuring aortic diameter with different MR techniques: comparison of three-dimensional (3D) navigated steady-state free-precession (SSFP), 3D contrast-enhanced magnetic resonance angiography (CE-MRA), 2D T2 black blood, and 2D cine SSFP. J Magn Reson Imaging JMRI 2010;31(1): 177–84.
21. Amano Y, Takahama K, Kumita S. Non-contrast-enhanced MR angiography of the thoracic aorta using cardiac and navigator-gated magnetization-prepared three-dimensional steady-state free precession. J Magn Reson Imaging JMRI 2008;27(3): 504–9.
22. Herborn CU, Watkins DM, Runge VM, et al. Renal Arteries: Comparison of Steady-State Free Precession MR Angiography and Contrast-enhanced MR Angiography. Radiology 2006; 239(1):263–8.
23. Maki JH, Wilson GJ, Eubank WB, et al. Steady-state free precession MRA of the renal arteries: breath-hold and navigator-gated techniques vs. CE-MRA. J Magn Reson Imaging JMRI 2007; 26(4):966–73.
24. Tao W, Shen Y, Guo L, et al. Role of non-contrast balanced steady-state free precession megnetic resonance angiography compared to contrast-enhanced megnetic resonance angiography in diagnosing renal artery stenosis: a meta-analysis. Chin Med J (Engl). 2014;127(19):3483–90.
25. Helyar VG, Gupta Y, Blakeway L, et al. Depiction of lower limb venous anatomy in patients undergoing interventional deep venous reconstruction-the role of balanced steady state free precession MRI. Br J Radiol 2018;91(1082):20170005.

Descargado para Anonymous User (n/a) en National Library of Health and Social Security de ClinicalKey.es por Elsevier en julio 13, 2023. Para uso personal exclusivamente. No se permiten otros usos sin autorización. Copyright ©2023. Elsevier Inc. Todos los derechos reservados.

26. Parker DL, Yuan C, Blatter DD. MR angiography by multiple thin slab 3D acquisition. Magn Reson Med 1991;17(2):434–51.
27. Davis WL, Blatter DD, Harnsberger HR, et al. Intracranial MR angiography: comparison of single-volume three-dimensional time-of-flight and multiple overlapping thin slab acquisition techniques. AJR Am J Roentgenol 1994;163(4): 915–20.
28. Goodrich KC, Blatter DD, Parker DL, et al. A quantitative study of ramped radio frequency, magnetization transfer, and slab thickness in three-dimensional time-of-flight magnetic resonance angiography in a patient population. Invest Radiol 1996;31(6):323–32.
29. Cavallo AU, Koktzoglou I, Edelman RR, et al. Noncontrast Magnetic Resonance Angiography for the Diagnosis of Peripheral Vascular Disease. Circ Cardiovasc Imaging 2019;12(5):e008844.
30. Drutman J, Gyorke A, Davis WL, et al. Evaluation of subclavian steal with two-dimensional phase-contrast and two-dimensional time-of-flight MR angiography. AJNR Am J Neuroradiol 1994;15(9):1642–5.
31. Hutter J, Grimm R, Forman C, et al. Highly undersampled peripheral Time-of-Flight magnetic resonance angiography: optimized data acquisition and iterative image reconstruction. Magma N Y N 2015;28(5):437–46.
32. Fushimi Y, Okada T, Kikuchi T, et al. Clinical evaluation of time-of-flight MR angiography with sparse undersampling and iterative reconstruction for cerebral aneurysms. NMR Biomed 2017;30(11). https://doi.org/10.1002/nbm.3774.
33. Sakata A, Fushimi Y, Okada T, et al. Evaluation of cerebral arteriovenous shunts: a comparison of parallel imaging time-of-flight magnetic resonance angiography (TOF-MRA) and compressed sensing TOF-MRA to digital subtraction angiography. Neuroradiology 2021;63(6):879–87.
34. HaiFeng L, YongSheng X, YangQin X, et al. Diagnostic value of 3D time-of-flight magnetic resonance angiography for detecting intracranial aneurysm: a meta-analysis. Neuroradiology 2017; 59(11):1083–92.
35. Ahmed SU, Mocco J, Zhang X, et al. MRA versus DSA for the follow-up imaging of intracranial aneurysms treated using endovascular techniques: a meta-analysis. J Neurointerventional Surg 2019; 11(10):1009–14.
36. Edelman RR, Sheehan JJ, Dunkle E, et al. Quiescent-interval single-shot unenhanced magnetic resonance angiography of peripheral vascular disease: Technical considerations and clinical feasibility. Magn Reson Med 2010;63(4):951–8.
37. Lombardi P, Carr JC, Allen BD, et al. Updates in Magnetic Resonance Venous Imaging. Semin Interv Radiol 2021;38(2):202–8.
38. Edelman RR, Carr M, Koktzoglou I. Advances in non-contrast quiescent-interval slice-selective (QISS) magnetic resonance angiography. Clin Radiol 2019;74(1):29–36.
39. Varga-Szemes A, Aherne EA, Schoepf UJ, et al. Free-Breathing Fast Low-Angle Shot Quiescent-Interval Slice-Selective Magnetic Resonance Angiography for Improved Detection of Vascular Stenoses in the Pelvis and Abdomen: Technical Development. Invest Radiol 2019;54(12):752–6.
40. Edelman RR, Giri S, Murphy IG, et al. Ungated radial quiescent-inflow single-shot (UnQISS) magnetic resonance angiography using optimized azimuthal equidistant projections: Ungated Quiescent-Inflow Single-Shot MRA. Magn Reson Med 2014;72(6):1522–9.
41. Koktzoglou I, Edelman RR. Radial Fast Interrupted Steady-State (FISS) Magnetic Resonance Imaging. Magn Reson Med 2018;79(4):2077–86.
42. Koktzoglou I, Huang R, Ong AL, et al. Feasibility of a sub-3-minute imaging strategy for ungated quiescent interval slice-selective MRA of the extracranial carotid arteries using radial k-space sampling and deep learning-based image processing. Magn Reson Med 2020;84(2):825–37.
43. Koktzoglou I, Gupta N, Edelman RR. Nonenhanced extracranial carotid MR angiography using arterial spin labeling: Improved performance with pseudo-continuous tagging. J Magn Reson Imaging 2011; 34(2):384–94.
44. Verma M, Pandey NN, Singh V, et al. A meta-analysis of the diagnostic performance of quiescent-interval-single-shot magnetic resonance angiography in peripheral arterial disease. Eur Radiol 2022;32(4):2393–403.
45. Lam A, Perchyonok Y, Ranatunga D, et al. Accuracy of non-contrast quiescent-interval single-shot and quiescent-interval single-shot arterial spin-labelled magnetic resonance angiography in assessment of peripheral arterial disease in a diabetic population. J Med Imaging Radiat Oncol 2020;64(1):35–43.
46. Salehi Ravesh M, Lebenatus A, Bonietzki A, et al. High-resolution, non-contrast-enhanced magnetic resonance angiography of the wrist, hand and digital arteries using optimized implementation of Cartesian quiescent interval slice selective (QISS) at 1.5 T. Magn Reson Imaging 2021;78:58–68.
47. LaBounty TM, Bhave N, Giri S, et al. Comparison of ileofemoral arterial access size between noncontrast 3T MR angiography and contrast-enhanced computed tomographic angiography in patients referred for transcatheter aortic valve replacement. J Magn Reson Imaging 2017;46(6):1847–50.
48. Cannaò PM, Muscogiuri G, Schoepf UJ, et al. Technical Feasibility of a Combined Noncontrast Magnetic Resonance Protocol for Preoperative

Descargado para Anonymous User (n/a) en National Library of Health and Social Security de ClinicalKey.es por Elsevier en julio 13, 2023. Para uso personal exclusivamente. No se permiten otros usos sin autorización. Copyright ©2023. Elsevier Inc. Todos los derechos reservados.

Transcatheter Aortic Valve Replacement Evaluation. J Thorac Imaging 2018;33(1):60–7.
49. Ferreira Botelho MP, Koktzoglou I, Collins JD, et al. MR imaging of iliofemoral peripheral vascular calcifications using proton density-weighted, in-phase three-dimensional stack-of-stars gradient echo: MRI of Iliofemoral Peripheral Vascular Calcifications. Magn Reson Med 2017; 77(6):2146–52.
50. Edelman RR, Silvers RI, Thakrar KH, et al. Nonenhanced MR angiography of the pulmonary arteries using single-shot radial quiescent-interval slice-selective (QISS): a technical feasibility study. J Cardiovasc Magn Reson 2017;19(1):48.
51. Salehi Ravesh M, Tesch K, Lebenatus A, et al. Clinical Value of Noncontrast-Enhanced Radial Quiescent-Interval Slice-Selective (QISS) Magnetic Resonance Angiography for the Diagnosis of Acute Pulmonary Embolism Compared to Contrast-Enhanced Computed Tomography and Cartesian Balanced Steady-State Free Precession. J Magn Reson Imaging 2020;52(5):1510–24.
52. Edelman RR, Giri S, Pursnani A, et al. Breath-hold imaging of the coronary arteries using Quiescent-Interval Slice-Selective (QISS) magnetic resonance angiography: pilot study at 1.5 Tesla and 3 Tesla. J Cardiovasc Magn Reson 2015;17:101.
53. Koktzoglou I, Murphy IG, Giri S, et al. Quiescent interval low angle shot magnetic resonance angiography of the extracranial carotid arteries: QLASH MRA of the Carotid Arteries. Magn Reson Med 2016;75(5):2072–7.
54. Koktzoglou I, Edelman RR. Super-resolution intracranial quiescent interval slice-selective magnetic resonance angiography. Magn Reson Med 2018; 79(2):683–91.
55. Shen D, Edelman RR, Robinson JD, et al. Single-Shot Coronary Quiescent-Interval Slice-Selective Magnetic Resonance Angiography Using Compressed Sensing: A Feasibility Study in Patients With Congenital Heart Disease. J Comput Assist Tomogr 2018;42(5):739–46.
56. Mostafa K, Pfarr J, Langguth P, et al. Clinical Evaluation of Non-Contrast-Enhanced Radial Quiescent-Interval Slice-Selective (QISS) Magnetic Resonance Angiography in Comparison to Contrast-Enhanced Computed Tomography Angiography for the Evaluation of Endoleaks after Abdominal Endovascular Aneurysm Repair. J Clin Med 2022;11(21):6551.
57. Miyazaki M, Sugiura S, Tateishi F, et al. Noncontrast-enhanced MR angiography using 3D ECG-synchronized half-Fourier fast spin echo. J Magn Reson Imaging JMRI 2000;12(5):776–83.
58. Lim RP, Storey P, Atanasova IP, et al. Three-dimensional electrocardiographically gated variable flip angle FSE imaging for MR angiography of the hands at 3.0 T: initial experience. Radiology 2009; 252(3):874–81.
59. Nakamura K, Miyazaki M, Kuroki K, et al. Noncontrast-enhanced peripheral MRA: Technical optimization of flow-spoiled fresh blood imaging for screening peripheral arterial diseases. Magn Reson Med 2011;65(2):595–602.
60. Urata J, Miyazaki M, Wada H, et al. Clinical evaluation of aortic diseases using nonenhanced MRA with ECG-triggered 3D half-Fourier FSE. J Magn Reson Imaging 2001;14(2):113–9.
61. Suga K, Ogasawara N, Okada M, et al. Lung perfusion impairments in pulmonary embolic and airway obstruction with non-contrast MR imaging. J Appl Physiol Bethesda Md 1985 2002;92(6):2439–51.
62. Ogasawara N, Suga K, Zaki M, et al. Assessment of lung perfusion impairment in patients with pulmonary artery-occlusive and chronic obstructive pulmonary diseases with noncontrast electrocardiogram-gated fast-spin-echo perfusion MR imaging. J Magn Reson Imaging JMRI 2004; 20(4):601–11.
63. Ward EV, Galizia MS, Usman A, et al. Comparison of quiescent inflow single-shot and native space for nonenhanced peripheral MR angiography. J Magn Reson Imaging JMRI 2013;38(6):1531–8.
64. Haneder S, Attenberger UI, Riffel P, et al. Magnetic resonance angiography (MRA) of the calf station at 3.0 T: intraindividual comparison of non-enhanced ECG-gated flow-dependent MRA, continuous table movement MRA and time-resolved MRA. Eur Radiol 2011;21(7):1452–61.
65. Lim RP, Hecht EM, Xu J, et al. 3D nongadolinium-enhanced ECG-gated MRA of the distal lower extremities: Preliminary clinical experience. J Magn Reson Imaging 2008;28(1):181–9.
66. Ono A, Murase K, Taniguchi T, et al. Deep vein thrombosis using noncontrast-enhanced MR venography with electrocardiographically gated three-dimensional half-Fourier FSE: preliminary experience. Magn Reson Med 2009;61(4):907–17.
67. Fan Z, Saouaf R, Liu X, et al. Non-Contrast MR Angiography: Flow-Sensitive Dephasing (FSD)-Prepared 3D Balanced SSFP. MAGNETOM Flash 2013;4:2–7.
68. Fan Z, Sheehan J, Bi X, et al. 3D noncontrast MR angiography of the distal lower extremities using flow-sensitive dephasing (FSD)-prepared balanced SSFP. Magn Reson Med 2009;62(6):1523–32.
69. Fan Z, Zhou X, Bi X, et al. Determination of the optimal first-order gradient moment for flow-sensitive dephasing magnetization-prepared 3D noncontrast MR angiography. Magn Reson Med 2011;65(4):964–72.
70. Fan Z, Hodnett PA, Davarpanah AH, et al. Noncontrast Magnetic Resonance Angiography of the Hand: Improved Arterial Conspicuity by Multidirectional

Descargado para Anonymous User (n/a) en National Library of Health and Social Security de ClinicalKey.es por Elsevier en julio 13, 2023. Para uso personal exclusivamente. No se permiten otros usos sin autorización. Copyright ©2023. Elsevier Inc. Todos los derechos reservados.

Flow-Sensitive Dephasing Magnetization Preparation in 3D Balanced Steady-State Free Precession Imaging. Invest Radiol 2011;46(8):515.
71. Lim RP, Fan Z, Chatterji M, et al. Comparison of Nonenhanced MR Angiographic Subtraction Techniques for Infragenual Arteries at 1.5 T: A Preliminary Study. Radiology 2013;267(1): 293–304.
72. Sheehan JJ, Fan Z, Davarpanah AH, et al. Nonenhanced MR Angiography of the Hand with Flow-Sensitive Dephasing–prepared Balanced SSFP Sequence: Initial Experience with Systemic Sclerosis. Radiology 2011;259(1):248–56.
73. Zhang N, Fan Z, Luo N, et al. Noncontrast MR angiography (MRA) of infragenual arteries using flow-sensitive dephasing (FSD)-prepared steady-state free precession (SSFP) at 3.0 Tesla: Comparison with contrast-enhanced MRA. J Magn Reson Imaging 2016;43(2):364–72.
74. Liu J, Zhang N, Fan Z, et al. Image Quality and Stenosis Assessment of Non-Contrast-Enhanced 3-T Magnetic Resonance Angiography in Patients with Peripheral Artery Disease Compared with Contrast-Enhanced Magnetic Resonance Angiography and Digital Subtraction Angiography. PLoS One 2016;11(11):e0166467.
75. Liu X, Fan Z, Zhang N, et al. Unenhanced MR angiography of the foot: initial experience of using flow-sensitive dephasing-prepared steady-state free precession in patients with diabetes. Radiology 2014;272(3):885–94.
76. Liu X, Zhang N, Fan Z, et al. Detection of infragenual arterial disease using non–contrast-enhanced MR angiography in patients with diabetes. J Magn Reson Imaging 2014;40(6):1422–9.
77. Wymer DT, Patel KP, Burke WF, et al. Phase-Contrast MRI: Physics, Techniques, and Clinical Applications. Radiographics 2020;40(1):122–40.
78. Stankovic Z, Allen BD, Garcia J, et al. 4D flow imaging with MRI. Cardiovasc Diagn Ther 2014; 4(2):173–92.
79. François CJ, Lum DP, Johnson KM, et al. Renal arteries: isotropic, high-spatial-resolution, unenhanced MR angiography with three-dimensional radial phase contrast. Radiology 2011;258(1): 254–60.
80. Hom JJ, Ordovas K, Reddy GP. Velocity-encoded Cine MR Imaging in Aortic Coarctation: Functional Assessment of Hemodynamic Events. Radiographics 2008;28(2):407–16.
81. Roldán-Alzate A, Francois CJ, Wieben O, et al. Emerging Applications of Abdominal 4D Flow MRI. AJR Am J Roentgenol 2016;207(1):58–66.
82. Azarine A, Garçon P, Stansal A, et al. Four-dimensional Flow MRI: Principles and Cardiovascular Applications. Radiographics 2019;39(3): 632–48.
83. Markl M, Schnell S, Barker AJ. 4D flow imaging: current status to future clinical applications. Curr Cardiol Rep 2014;16(5):481.
84. Neuhaus E, Weiss K, Bastkowski R, et al. Accelerated aortic 4D flow cardiovascular magnetic resonance using compressed sensing: applicability, validation and clinical integration. J Cardiovasc Magn Reson 2019;21(1):65.
85. Pathrose A, Ma L, Berhane H, et al. Highly accelerated aortic 4D flow MRI using compressed sensing: Performance at different acceleration factors in patients with aortic disease. Magn Reson Med 2021;85(4):2174–87.
86. de Boer A, Villa G, Bane O, et al. Consensus-Based Technical Recommendations for Clinical Translation of Renal Phase Contrast MRI. J Magn Reson Imaging 2022;55(2):323–35.
87. Youn SW, Lee J. From 2D to 4D Phase-Contrast MRI in the Neurovascular System: Will It Be a Quantum Jump or a Fancy Decoration? J Magn Reson Imaging 2022;55(2):347–72.
88. Dyverfeldt P, Bissell M, Barker AJ, et al. 4D flow cardiovascular magnetic resonance consensus statement. J Cardiovasc Magn Reson 2015;17(1): 72.
89. Zhong L, Schrauben EM, Garcia J, et al. Intracardiac 4D Flow MRI in Congenital Heart Disease: Recommendations on Behalf of the ISMRM Flow & Motion Study Group. J Magn Reson Imaging 2019;50(3):677–81.
90. Oechtering TH, Roberts GS, Panagiotopoulos N, et al. Abdominal Applications of Quantitative 4D Flow MRI. Abdom Radiol N Y 2022;47(9):3229–50.
91. Shin T, Hu BS, Nishimura DG. Off-resonance-robust velocity-selective magnetization preparation for non-contrast-enhanced peripheral MR angiography. Magn Reson Med 2013;70(5): 1229–40.
92. de Rochefort L, Maître X, Bittoun J, et al. Velocity-selective RF pulses in MRI. Magn Reson Med 2006;55(1):171–6.
93. Qin Q, Shin T, Schär M, et al. Velocity-Selective Magnetization-Prepared Non-Contrast-Enhanced Cerebral MR Angiography at 3T: Improved Immunity to B0/B1 Inhomogeneity. Magn Reson Med 2016;75(3):1232–41.
94. Zhu D, Li W, Liu D, et al. Non-contrast-enhanced abdominal MRA at 3 T using velocity-selective pulse trains. Magn Reson Med 2020;84(3): 1173–83.
95. Shin T, Menon RG, Thomas RB, et al. Unenhanced Velocity-Selective MR Angiography (VS-MRA): Initial Clinical Evaluation in Patients With Peripheral Artery Disease. J Magn Reson Imaging 2019;49(3): 744–51.
96. Edelman RR, Siewert B, Adamis M, et al. Signal targeting with alternating radiofrequency (STAR)

Descargado para Anonymous User (n/a) en National Library of Health and Social Security de ClinicalKey.es por Elsevier en julio 13, 2023. Para uso personal exclusivamente. No se permiten otros usos sin autorización. Copyright ©2023. Elsevier Inc. Todos los derechos reservados.

sequences: application to MR angiography. Magn Reson Med 1994;31(2):233–8.
97. Zhang LJ, Peng J, Wen J, et al. Non-contrast-enhanced magnetic resonance angiography: a reliable clinical tool for evaluating transplant renal artery stenosis. Eur Radiol 2018;28(10): 4195–204.
98. Sebastià C, Sotomayor AD, Paño B, et al. Accuracy of unenhanced magnetic resonance angiography for the assessment of renal artery stenosis. Eur J Radiol Open 2016;3:200–6.
99. Braidy C, Daou I, Diop AD, et al. Unenhanced MR angiography of renal arteries: 51 patients. AJR Am J Roentgenol 2012;199(5):W629–37.
100. Albert TSE, Akahane M, Parienty I, et al. An international multicenter comparison of time-SLIP unenhanced MR angiography and contrast-enhanced CT angiography for assessing renal artery stenosis: the renal artery contrast-free trial. AJR Am J Roentgenol 2015;204(1):182–8.
101. Parienty I, Rostoker G, Jouniaux F, et al. Renal artery stenosis evaluation in chronic kidney disease patients: nonenhanced time-spatial labeling inversion-pulse three-dimensional MR angiography with regulated breathing versus DSA. Radiology 2011;259(2):592–601.
102. Liang KW, Chen JW, Huang HH, et al. The Performance of Noncontrast Magnetic Resonance Angiography in Detecting Renal Artery Stenosis as Compared With Contrast Enhanced Magnetic Resonance Angiography Using Conventional Angiography as a Reference. J Comput Assist Tomogr 2017;41(4):619–27.
103. Bley TA, François CJ, Schiebler ML, et al. Noncontrast-enhanced MRA of renal artery stenosis: validation against DSA in a porcine model. Eur Radiol 2016;26(2):547–55.
104. Shimada K, Isoda H, Okada T, et al. Noncontrast-enhanced MR portography with time-spatial labeling inversion pulses: Comparison of imaging with three-dimensional half-fourier fast spin-echo and true steady-state free-precession sequences. J Magn Reson Imaging 2009;29(5): 1140–6.
105. Shimada K, Isoda H, Okada T, et al. Non-contrast-enhanced MR angiography for selective visualization of the hepatic vein and inferior vena cava with true steady-state free-precession sequence and time-spatial labeling inversion pulses: Preliminary results. J Magn Reson Imaging 2009;29(2): 474–9.
106. Shimada K, Isoda H, Okada T, et al. Non-contrast-enhanced hepatic MR angiography with true steady-state free-precession and time spatial labeling inversion pulse: optimization of the technique and preliminary results. Eur J Radiol 2009; 70(1):111–7.
107. Ohno T, Isoda H, Furuta A, et al. Non-contrast-enhanced MR portography and hepatic venography with time-spatial labeling inversion pulses: comparison at 1.5 Tesla and 3 Tesla. Acta Radiol Open 2015;4(5). 2058460115584110.
108. Atanasova IP, Kim D, Lim RP, et al. Noncontrast MR angiography for comprehensive assessment of abdominopelvic arteries using quadruple inversion-recovery preconditioning and 3D balanced steady-state free precession imaging. J Magn Reson Imaging JMRI 2011;33(6):1430–9.
109. Satogami N, Okada T, Koyama T, et al. Visualization of external carotid artery and its branches: non-contrast-enhanced MR angiography using balanced steady-state free-precession sequence and a time-spatial labeling inversion pulse. J Magn Reson Imaging JMRI 2009;30(3):678–83.
110. Okuaki T, Ishimoto T, Miyati T, et al. Separate pulmonary artery and vein magnetic resonance angiography by use of an arterial spin labeling method. Radiol Phys Technol 2014;7(2):352–7.
111. Eddleman CS, Jeong HJ, Hurley MC, et al. 4D radial acquisition contrast-enhanced MR angiography and intracranial arteriovenous malformations: quickly approaching digital subtraction angiography. Stroke 2009;40(8):2749–53.
112. Suzuki Y, Fujima N, van Osch MJP. Intracranial 3D and 4D MR Angiography Using Arterial Spin Labeling: Technical Considerations. Magn Reson Med Sci 2020;19(4):294–309.
113. Rojas-Villabona A, Pizzini FB, Solbach T, et al. Are Dynamic Arterial Spin-Labeling MRA and Time-Resolved Contrast-Enhanced MRA Suited for Confirmation of Obliteration following Gamma Knife Radiosurgery of Brain Arteriovenous Malformations? AJNR Am J Neuroradiol 2021;42(4): 671–8.
114. Jensen-Kondering U, Lindner T, van Osch MJP, et al. Superselective pseudo-continuous arterial spin labeling angiography. Eur J Radiol 2015; 84(9):1758–67.
115. Fujima N, Osanai T, Shimizu Y, et al. Utility of noncontrast-enhanced time-resolved four-dimensional MR angiography with a vessel-selective technique for intracranial arteriovenous malformations. J Magn Reson Imaging JMRI 2016; 44(4):834–45.
116. Suzuki Y, Helle M, Koken P, et al. Simultaneous acquisition of perfusion image and dynamic MR angiography using time-encoded pseudo-continuous ASL. Magn Reson Med 2018;79(5): 2676–84.
117. Altes TA, Mai VM, Munger TM, et al. Pulmonary embolism: comprehensive evaluation with MR ventilation and perfusion scanning with hyperpolarized helium-3, arterial spin tagging, and contrast-

Descargado para Anonymous User (n/a) en National Library of Health and Social Security de ClinicalKey.es por Elsevier en julio 13, 2023. Para uso personal exclusivamente. No se permiten otros usos sin autorización. Copyright ©2023. Elsevier Inc. Todos los derechos reservados.

enhanced MRA. J Vasc Interv Radiol JVIR 2005; 16(7):999–1005.
118. Wang J, Börnert P, Zhao H, et al. Simultaneous noncontrast angiography and intraplaque hemorrhage (SNAP) imaging for carotid atherosclerotic disease evaluation. Magn Reson Med 2013;69(2): 337–45.
119. Ginami G, Lòpez K, Mukherjee RK, et al. Non-contrast enhanced simultaneous 3D whole-heart bright-blood pulmonary veins visualization and black-blood quantification of atrial wall thickness. Magn Reson Med 2019;81(2):1066–79.
120. Li D, Qiao H, Han Y, et al. Histological validation of simultaneous non-contrast angiography and intraplaque hemorrhage imaging (SNAP) for characterizing carotid intraplaque hemorrhage. Eur Radiol 2021;31(5):3106–15.
121. Li D, Zhao H, Chen X, et al. Identification of intraplaque haemorrhage in carotid artery by simultaneous non-contrast angiography and intraPlaque hemorrhage (SNAP) imaging: a magnetic resonance vessel wall imaging study. Eur Radiol 2018;28(4):1681–6.

Descargado para Anonymous User (n/a) en National Library of Health and Social Security de ClinicalKey.es por Elsevier en julio 13, 2023. Para uso personal exclusivamente. No se permiten otros usos sin autorización. Copyright ©2023. Elsevier Inc. Todos los derechos reservados.